https://doi.org/10.5194/egusphere-2026-1720
Preprint. Discussion started: 8 April 2026

DMS, MeSH and nanoparticles in semi-controlled deck-borne experiments using Antarctic seawater: on the effect of UV light

Guillaume Chamba[1], Karine Sellegri[1], Valérie Gros[2], Clémence Rose[1], Leah Williams[3], Elisa Berdalet[4], Dolors Vaqué[4], Magda Vila[4], Queralt Güell-Bujons[4], Elisabet-Laia Sà[4], Yaiza M. Castillo[4], Arianna Rocchi[4], Aurélie Colomb[1], Jean-Marc Pichon[1], Mickaël Ribeiro[1], Charel Wohl[4,5,6], Manuel Dall'Osto[4] and Rafel Simó[4]

[1] Laboratoire de Météorologie Physique, CNRS UMR 6016, Université Clermont Auvergne, avenue Blaise Pascal, Aubière, France
[2] Laboratoire des Sciences du Climat et de l'Environnement, CNRS-CEA-UVSQ, IPSL, 91 191 Gif sur Yvette, France
[3] Aerodyne Research, Billerica, MA 01821, USA
[4] Institut de Ciències del Mar (ICM-CSIC), Passeig Marítim de la Barceloneta, 37-49, 08003 Barcelona, Catalonia, Spain
[5] Centre of Ocean and Atmospheric Sciences, University of East Anglia, Norwich, UK
[6] National Centre for Atmospheric Science, University of East Anglia, Norwich, UK

Correspondence to: Karine Sellegri (k.sellegri@opgc.fr) and Rafel Simó (rsimo@icm.csic.es)

Abstract. Sulfur-containing volatile organic compounds (VOCs) such as dimethyl sulfide (DMS) and methanethiol (MeSH) are are of particular interest among oceanic VOCs emitted by the ocean, both for their central role in the marine sulfur cycle and as potential precursors to secondary aerosol formation. However, the quantification of DMS and MeSH emissions as a function of biological components of the ocean under variable environmental factors are still too scarce for reliable future predictions. In this study we report on measurements of DMS, MeSH and nanoparticle concentrations in the headspace of two on-deck Air-Sea Interface Tanks (ASITs). The cover of one ASIT prevented the transmission of UV light below 380 nm in wavelength and we report on the effect of UV light on fluxes and concentrations. These measurements were carried out near the Antarctic Peninsula during the POLAR-CHANGE campaign in summer 2023. Air-sea fluxes inside the ASITs were always positive, i.e. degassing from seawater to air, with DMS and MeSH fluxes averaging 3.03 pmol·m^{-2}·s^{-1} ($F_{ASIT\text{-}DMS}$) and 0.64 pmol·m^{-2}·s^{-1} ($F_{ASIT\text{-}MeSH}$), respectively. DMS emission did not vary significantly between day and night, but the ratio $F_{ASIT\text{-}MeSH}/(F_{ASIT\text{-}DMS} + F_{ASIT\text{-}MeSH})$ showed a clear maximum at night and a decrease over daytime. Calculated aqueous DMS concentrations showed maxima in the open Southern Ocean north of the Antarctic Peninsula (2.5-3 nM), minima in the Marginal Ice Zone (MIZ) in the Weddell Sea (1 nM) and moderate values along the western coast of the peninsula (around 1.5-2 nM). Cryptophytes, nanophytoplankton, and bacterial concentrations showed positive correlations with calculated aqueous DMS and MeSH concentrations during two experiments when seawater was held in the ASITs for two days. Removal of UV light increased DMS fluxes by 24% and MeSH fluxes by 58%. New particle formation occurred only in the absence of UV-light. Interestingly, the highest impact of UV removal, especially on increased MeSH emission, was seen during the night suggesting a lag period between the exposure and the physiological response of the cells. UV light caused slight phytoplankton light stress at noon, which negatively affected the short-term growth of nanophytoplankton in the ASIT, especially in open Southern Ocean waters.

1 Introduction

Various volatile organic compounds (VOCs) are emitted from the surface of the ocean and are now considered key in understanding marine-atmosphere interactions and atmospheric chemistry. Among the wide variety of VOCs emitted by the oceans, sulfur-containing compounds such as dimethyl sulfide (DMS) and methanethiol (MeSH) can be particularly important due to their prominent role in the marine sulfur cycle as they represent the

https://doi.org/10.5194/egusphere-2026-1720
Preprint. Discussion started: 8 April 2026

main natural source to the atmosphere (Andreae, 1990; Bates et al., 1992). Also, the role of DMS in marine aerosol formation processes via its oxidation to form sulfur dioxide (SO_2), sulfuric acid (H_2SO_4) and methanesulfonic acid (MSA), make it a key compound in the study of the marine atmosphere and in the link to the formation of new particles in the CLAW hypothesis (Charlson et al.,1987). The significance of MeSH has only recently gained attention. MeSH is often emitted alongside DMS, is more reactive than DMS and represents an additional contribution to the atmospheric sulfur budget (Novak et al., 2022). However, MeSH is far less understood than DMS in terms of production pathways and atmospheric fate (Lawson et al., 2020; Novak et al., 2022). Recent studies using atmospheric models have shown that including MeSH emissions and chemistry alongside DMS might increase the aerosol cooling effect, especially in the southern oceans (Novak et al., 2022; Wohl et al., 2024).

DMS and MeSH are mainly produced in the oceans through degradation of dimethylsulfoniopropionate (DMSP) by phytoplankton and bacteria via cleavage (giving rise to DMS) or demethylation (producing MeSH) (Kiene et al., 2000; Carpenter et al., 2012). DMSP is synthesized by various organisms including phytoplankton (mainly dinoflagellates and haptophytes), heterotrophic bacteria and macro-algae, and subsequently exuded or released in seawater through viral lysis, grazing or senescence (Asher et al., 2017, Jackson and Gabric, 2022, Shaw et al., 2022, Vaqué et al., 2025).

The formation of new aerosol particles induced by oxidation of sulfur compounds into condensable products is expected to be particularly important in the Southern Ocean, where DMS and MeSH emissions are elevated during the austral summer and clearly exceed emissions and transport of aerosol precursors from distant inhabited and exposed land masses (Joge et al., 2025). Also, the Southern Ocean is a key region for climate regulation on Earth, and one that is undergoing rapid transformations due to climate change with its related associated processes including increased freshwater input from ice melt, ocean warming, alterations in water column stratification, nutrient cycling and marine life exposure to UV radiation (Constable et al., 2022; Sallée et al., 2021). These changes are affecting plankton community structure and productivity and therefore are expected to alter organic matter production and consumption as well as the production of biogenic VOCs like DMS and MeSH (Häder et al., 2007; Hernando et al., 2020; Latorre et al., 2023). In particular, changes in the abundance or species composition of nanophytoplankton, cryptophytes, and bacteria, known contributors to DMSP production and cycling, may shift the regional sulfur emissions profile (Stefels et al., 2007; McParland & Levine, 2019).

In view of these factors, several points remain to be clarified, such as the quantification of VOC emissions and their integration into modelling tools. Rocco et al. (2025a) evidenced a relationship between seawater DMS concentrations and nanophytoplankton cell abundance in enclosure experiments incubating a range of plankton communities from the Southwest Pacific Ocean. In that study, as in many previous ones, DMS was not correlated to Chl-a, the commonly used tracer for phytoplankton biomass. Instead, the positive correlation of DMS to nanophytoplankton cell abundance was found useful for predicting atmospheric DMS concentrations (Salignat et al., 2025). However, the relationship evidenced by Rocco et al. (2025a) needs to be tested in other contrasted environments. Also, a better understanding of the fate of both DMS and MeSH in terms of reactivity and formation of new aerosol particles in the open ocean marine atmosphere requires additional research.

In this study we report on measurements of airborne DMS, MeSH, calculation of their air-sea fluxes and aqueous concentrations, and measurements of aerosol nanoparticle concentrations, all within on-deck Air-Sea Interface Tanks (ASITs) exposed to natural or eliminated UV light. These measurements were carried out in coastal and open seawaters near the Antarctic Peninsula and the Weddell Sea during the POLAR-CHANGE cruise in February–March 2023.

2 Material and methods

2.1 Experimental strategy and set-up

https://doi.org/10.5194/egusphere-2026-1720
Preprint. Discussion started: 8 April 2026

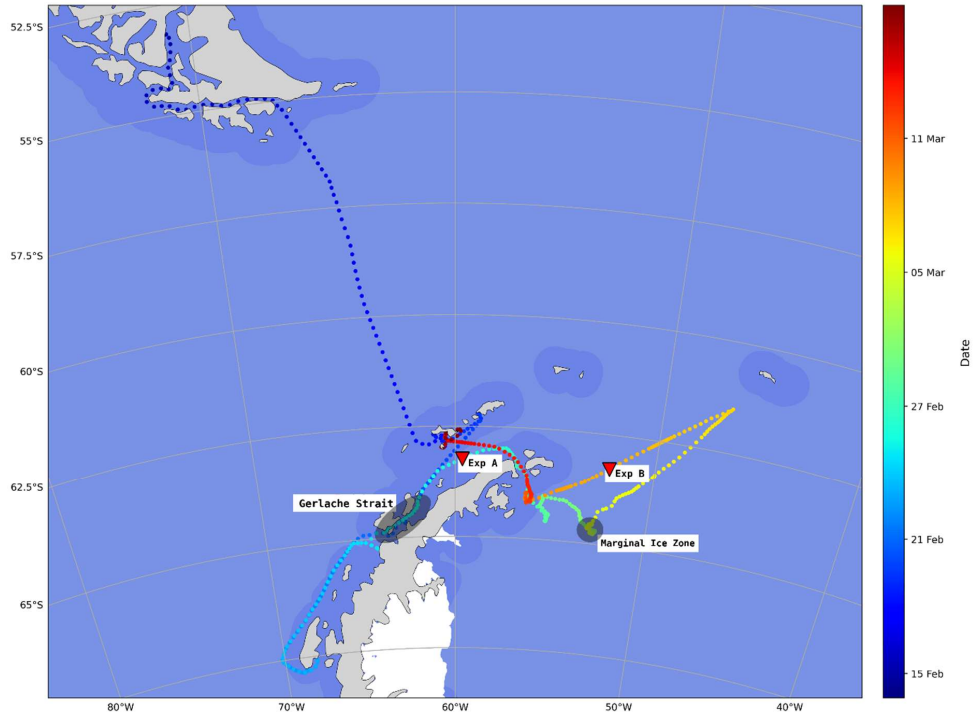

Figure 1: POLAR-CHANGE cruise track and location of the A and B ASIT experiments. The track colour (colour bar) indicates the sampling period, and the darker blue areas in the background indicate 100 km distance from the coast. Red triangles indicate the sampling location of each experiment. Transparent grey area refers to specific locations discussed in the text.

The air and seawater data in this study were collected during the POLAR-CHANGE cruise, which was conducted from 14 February to 17 March 2023 aboard the B.I.O. *Hespérides* around the Antarctic Peninsula and in the northern Weddell Sea. Data from this campaign were obtained from two main areas visited on different periods (Fig. 1): i) near the coast of the Antarctic Peninsula and the Antarctic islands, referred to as *coastal*, and ii) farther offshore, referred to as *open ocean*. The definition of the two areas were arbitrarily set by a 100 km limit from the coast. Two ASIT enclosure experiments were conducted, (A) in coastal waters and (B) in open ocean waters (Fig. 1).

The experimental setup was similar to that described in Sellegri et al. (2023). It consisted of two Air-Sea Interface Tanks (ASITs) installed on deck and connected to a set of air analysis instruments installed in a container close to the tanks (detailed description below) (Fig. 2). The tanks, with a total volume of 1.8 m³, were half-filled with seawater pumped to the ASITs from a 4m depth (see details below). A continuous flow of clean aerosol-free air at 25 L min^{-1} was introduced into each of the ASITs via a flushing line, resulting in a residence time of 40 minutes. The outflows from the ASITs (purple and red lines, Fig. 2) were connected to the analytical instruments set via a four-way valve that switched every 20 minutes, allowing alternate measurements of the air from both ASITs, as well as the incoming air (from the flushing line; green line, Fig. 2), and the ambient air (yellow line, Fig. 2). During the POLAR-CHANGE cruise, one ASIT was covered with a lid transparent to all radiation wavelengths (Control-ASIT), while the other was covered with a lid blocking UV wavelengths below 380 nm i.e. removing UV light exposure inside the ASIT (noUV-ASIT) (Fig. S.1).

https://doi.org/10.5194/egusphere-2026-1720
Preprint. Discussion started: 8 April 2026

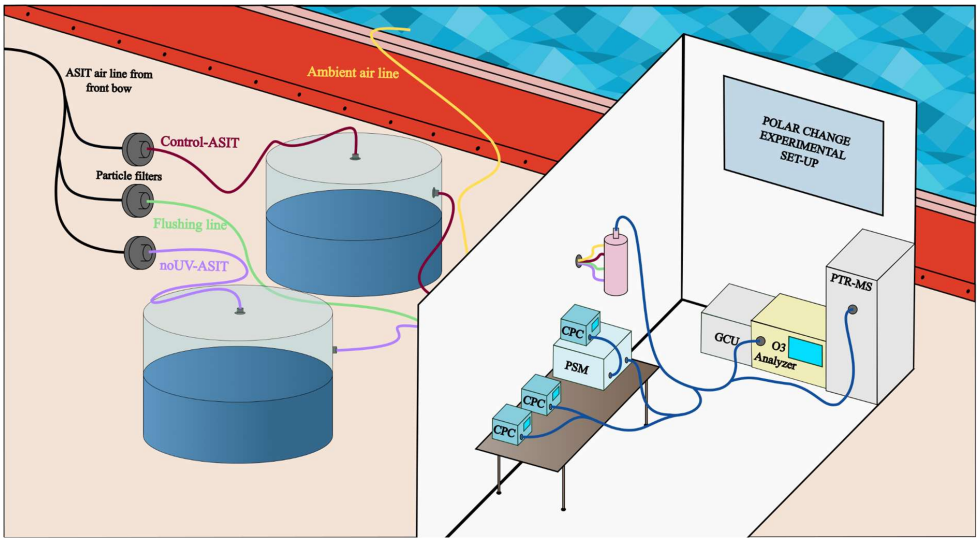

Figure 2: ASIT experimental set-up in the POLAR-CHANGE cruise (as in Sellegri et al., 2023).

The ASIT headspace was continuously flushed with particle-free (filtered) air. In contrast, the lower section containing seawater was operated either in a *continuous flow mode* or in a *static mode* without water renewal. The *continuous mode* was used during most of the cruise with seawater pumped to the ASITs from a 4m depth and flushed out with an average water residence time of approximately 6 hours. The *static flow mode* was applied in the two Experiments, A and B, in which the water remained incubated in the ASITs for two days.

To characterize the seawater entering the ASITs in *continuous flow mode*, samples were collected from the ship's underway water outlet on deck every 6 - 12 hours (i.e. 2 to 4 times per day) throughout the entire cruise. This outlet was derived from the same intake water used to fill the ASITs. During experiments A and B, discrete water samples were also collected every 6 hours from inside the ASITs (using a tap designed for this purpose), to monitor biological changes in the enclosed natural communities and to identify potential effects from UV light exposure. Cell abundances of microbial groups were estimated by combining flow cytometry and optical and fluorescence microscopy (described below).

2.2 Headspace characterization

The outgoing air line from the ASITs was connected to a set of instruments. An Ozone Analyzer (Thermo Scientific Model 49i) was used to monitor ozone. A Proton Transfer Reaction Quadrupole Mass Spectrometer (PTR-QMS, Ionicon) was used for VOC concentrations including DMS and MeSH. It was operated in standard conditions (Table S.1) and provided a E/N ratio of about 130 Td (with E the electric field strength and N the gas number density, 1 Td = 10^{-17} V cm^{-2}). Table S.2 gives the m/z monitored during the campaign, with the tentative name of the corresponding compound. As the mass resolution of the PTR-QMS is unit mass, we cannot rule out that interfering compounds were detected at the same m/z. However, the very good correlations found between MeSH concentrations and DMS concentrations, and between sea–air MeSH fluxes and DMS fluxes (Fig. 5), give good confidence to the mass attribution to the target compounds. A Gas Calibration Unit (Ionicon) was used for daily background instrument determination (catalyzer heated at 350 °C) and calibration. Three calibrations with an NPL (National Physics Laboratory, Teddington, UK) standard (including DMS) were made on-board and showed good stability of the instrument. Average instrument sensitivity for the different compounds is presented in Table S.2.The Minimum Limit of Detection (MLD) was determined from the standard deviation of blank measurements, following the method described in Rocco et al. (2025a).

https://doi.org/10.5194/egusphere-2026-1720
Preprint. Discussion started: 8 April 2026

Sea–air fluxes in the ASITs were calculated based on the difference in concentration between the flushing air and the ASIT outflow, using the following equation:

$$F_{ASIT-x} = Q \times \frac{C_{ASIT} - C_{flush}}{A} \quad (1)$$

where F_{ASIT-x} (mol·m^{-2}·s^{-1}) is the net flux of the compound from the water to the air, Q (m^3·s^{-1}) is the air volume flow rate in the ASITs, C_{ASIT} (mol·m^{-3}) is the concentration of the compound in the air leaving the ASIT, C_{flush} (mol·m^{-3}) is the concentration in the flush air entering the ASIT. A (m^2) is the water surface area in the ASIT. Using comparisons between measured fluxes and their prediction from empirical relationships using measured seawater dissolved DMS concentrations, SST and windspeed, Rocco et al. (2025a) calculated that the ASIT system generated fluxes equivalent to open ocean 2 m·s^{-1} wind speed fluxes.

Particle concentrations were measured using several Condensation Particle Counters (CPCs), including two from TSI (Models 3010 and 3772) and a water CPC (MAGIC 200/210, Aerosol Devices). A Particle Size Magnifier (PSM, Airmodus A11) coupled to a CPC was also used in stepping mode. The particle counters provided concentrations with four cutoff diameters: 1 and 3 nm using the PSM, 5 nm using the MAGIC CPC, and 10 nm using the TSI CPCs. Loss corrections in the tubing were calculated according to the equation from Willeke and Baron (1993). The correction for the concentration of 1-3 nm particles (N_{1-3}) was made by considering an average diameter of 2 nm, and for 1-10 nm particles (N_{1-10}), by taking an average diameter of 3 nm. According to our analyses of the particle size distribution, this correction results in a slight overestimation of losses, which are generally smaller than estimated here. The formation rate of new particles was calculated with the following equation:

$$J = \frac{dC_{ASIT}}{dt} - \frac{Q \times C_{flush}}{V} \quad (2)$$

where J (particles m^{-3}·s^{-1}) is the rate of formation of new particles, C_{ASIT} (particles·m^{-3}) is the concentration of particles in the air exiting the ASIT and C_{flush} (particles·m^{-3}) is the concentration of particles in the flush air entering the ASIT. Yet, the contribution of the second term, which corresponds to the contribution of particles entering the ASITs, is minimal due to the use of a particles filter on the flushing line. In the calculations of formation rates in the following sections, the concentrations taken will be those of particles greater than 1 nm (N_1) corrected for diffusion losses in the lines. t is time in seconds, Q (m^3·s^{-1}) is the inlet flow into the ASITs in and V (m^3) is the volume of the headspace in the ASITs.

The flushing air line for the ASITs was sourced from the bow of the vessel to avoid contamination from engine and kitchen exhausts as the ship moved forward. Data from the air lines were filtered for two hours after contamination events, which were identified based on elevated levels of ozone, benzene, and xylene, as well as changes in particle size distribution ($N_{10} > 0.5 \times N_1$) and variability in particle concentration during a 20-minute measurement period.

Seawater concentrations of DMS in the ASIT (DMS_w) were calculated according to the hypothesis that the headspace DMS concentrations (DMS_{air}) partially reached Henry's law equilibrium, as determined in the Rocco et al. (2025a) study that used the same system. DMS_w was calculated using:

$$DMS_w = DMS_{air} \times f_{sal} \times H^{cc}_{s(T)} \times 2.6 \quad (3)$$

where f_{sal} is a dimensionless factor accounting for the effect of salinity on solubility (f_{sal} = 0.848 for DMS, determined experimentally by Dacey et al., 1984) and 2.6 is the deviation from Henry's law equilibrium determined with DMS_w and DMS_{air} measurements in Rocco et al. (2025a). $H_s^{cc}{}_{(T)}$ is the dimensionless Henry's law solubility expressed as concentration in water over concentration in air and is a function of temperature (T) (Sander et al., 2023). $MeSH_w$ was calculated the same way but the deviation from Henry's law equilibrium was established to 7.2 by other measurements within the POLAR-CHANGE campaign (Wohl & Williams et al., in review; Fig. S7).

https://doi.org/10.5194/egusphere-2026-1720
Preprint. Discussion started: 8 April 2026

2.3 Seawater biological parameters

Chlorophyll-a. Between 200 and 750 mL of seawater were filtered through 25 mm Whatman GF/F glass fibre filters. All filters were stored at -20 °C until analyses on board the R/V Hesperides. Chlorophyll-a (Chl-a) concentrations were estimated fluorometrically after extraction in 90 % acetone at 4 ºC for 24h (Yentsch and Menzel, 1963). Readings were conducted on a Turner 10AU fluorimeter calibrated with pure chlorophyll extract from spinach (Sigma C5357) using a Beckton-Dickinson spectrophotometer.

Viral Abundance. Seawater subsamples (2 mL) were fixed with glutaraldehyde (0.5 % final concentration), kept at 4 °C for 15–30 min in the dark, flash-frozen in liquid nitrogen and finally stored at -80 °C until analysis, as described in Brussaard (2004). Viral counts were conducted in a Cytoflex flow cytometer at the ICM-CSIC laboratory (up to 5 months after sampling). Samples were diluted with TE-buffer (10:1 mM Tris: EDTA), stained with 50x SYBR Green I to a final concentration of 1 %, heated in an 80 ºC bath for 10 min and run at a constant flow rate of 60 µL min^{-1} according to Brussaard (2004). Viruses were determined in bivariate scatter plots of the green fluorescence of stained nucleic acids *versus* side scatter (Brussaard 2004). Depending on their green fluorescent and side scatter signals, we identified three distinct virus populations (V1-V3), and a fourth population in some of the samples (V4). Presumably, V1 and V2 populations are considered to be dominated by bacteriophages (Biggs et al., 2021). The V3-V4 fractions generally contain eukaryotic algal viruses (Evans et al. 2009).

Bacterial abundance. Seawater subsamples (2 mL) were fixed with 1 % paraformaldehyde + 0.05 % glutaraldehyde for bacteria estimations by flow cytometry. After 15–30 min in the dark at 4 °C, the fixed samples were flash-frozen in liquid nitrogen and subsequently stored at -80 °C. Bacterial abundances (Gasol and Del Giorgio, 2000) were measured in a Cytoflex flow cytometer at the ICM-CSIC laboratory (up to 5 months after sampling). On the day of analysis, samples were thawed, stained with 50x SYBR Green I at a final 1 % concentration and incubated for 5 min in the dark. Based on the flow cytometer side scatter versus green fluorescence (FL1) signatures, with high nucleic acid (HNA, considered active) from low nucleic acid (LNA, comparatively less active or dormant) content bacteria were identified.

Pico- and nanophytoplankton abundance. Samples for photosynthetic pico- and nanophytoplankton abundances were collected on 5 mL cryovials, fixed with glutaraldehyde (1% final concentration) and frozen in liquid nitrogen following Vaulot et al., (1989). Cell abundances were detected with a 488 nm laser beam from their signatures in a plot of side scatter (SSC) versus green fluorescence (FL3), separating the picophytoplankton fraction of 1–2 µm (sphere equivalent diameter, SED), the nanophytoplankton fractions of SEDs of 2–7 µm, 7–15 µm, 15–20 µm and the Cryptophytes size classes (*Cryptomonas* spp., identified by their phycoerythrin signal in the FL3 vs orange fluorescence FL2 plots).

Nanoflagellate abundance. Abundances of heterotrophic and phototrophic nanoflagellates, including *Phaeocystis*, in the size fraction 2–20 µm (SED) were determined by epifluorescence microscopy (Olympus BX40-102/E at 1000X). Subsamples of 30 mL were taken from seawater, fixed with glutaraldehyde (1 % final concentration), filtered through 0.6 µm black (25 mm diameter) polycarbonate filters, and stained with 4,6-diamidino-2-phenylindole (DAPI) at a final concentration of 5 µg mL-1 (Sieracki et al., 1985). Counts of heterotrophic nanoflagellates (HNFs) and phototrophic nanoflagellates (PNFs) were conducted using an UV excitation filter (BP 360–370 nm) and barrier filter (BA 420–460 nm) and with a blue wavelength excitation filter (bandpass (BP) 460–490 nm) and barrier (emission) filter (BA; 510–550 nm). PNFs were distinguished under the blue light by the observation of red fluorescence emitted by photosynthetic plastid structures. At least 50 HNFs and 50 PNFs were counted per sample (3 transects of 5 mm in each filter) and classified into ≤ 2 µm, 2–5 µm, 5–10 µm, and 10–20 µm size (SED) classes.

Photosynthetic efficiency. The relative efficiency of excitation energy captured by the photosystem II (PSII), calculated as Fv/Fm, is used as a proxy of phytoplankton stress and fitness (Gorbunov et al., 2020; Gorbunov and Falkowski, 2022). The metric is measured by a multi-color fluorescence induction and relaxation instrument (mini-FIRe) (Gorbunov et al., 2020). The instrument records two parameters: F_0 as the minimal yield of

https://doi.org/10.5194/egusphere-2026-1720
Preprint. Discussion started: 8 April 2026

fluorescence before fast light flashes, and F_m, the maximum yield of fluorescence due to the reradiation of the maximum number of photons. The difference between F_m and F_0 is called variable fluorescence (F_v). The quotient of F_v/F_m represents the effective photosynthetic efficiency of the community measured under light conditions (Gorbunov and Falkowski, 2022). F_v/F_m has no units, so that it is independent of the phytoplankton abundance and allows comparisons between environments. Aliquots of 10 mL were sampled from the underway system and the ASITs and rapidly placed in the chamber of the mini-FIRe to apply the induction and relaxation protocol for dilute samples. No dark acclimation period was used. A hundred acquisitions were averaged for each sample using the *fview* software and the resulting data was processed with the *fprope* software to obtain all the desired parameters.

3 Results

3.1 Gas-phase concentrations and air-sea fluxes in the ASITs

Out of the 22 compounds monitored by the PTR-QMS, only two, DMS and MeSH, were found to be enriched in the ASITs headspace with respect to the entering flushing air. No enrichment of benzene, toluene, ethylbenzene and xylene (BTEX), monoterpenes, isoprene, or iodomethane were detected in the ASITs headspace, as the same concentrations were observed at the inlet (i.e., in the flushing line) and the outlet (typically 0.13, 0.057, 0.05, and 0.1 ppb, respectively), differing from previous observations using this set-up with different seawaters (Rocco et al. 2021; Rocco et al., 2025b). The most plausible explanation for the lack of emissions is the concentrations of these compounds in the aqueous phase were below detection limits, combined with cold seawater and the absence of wind friction (low equivalent wind speeds) in the ASITs.

Ozone concentrations in the ambient air varied between 5 and over 20 ppb (Fig. 3) throughout the cruise with an average around 15 ppb. In contrast, ozone concentrations in the flushing line and the ASIT outlets were significantly lower, averaging around 7 ppb, primarily due to losses along the sampling line from the bow of the vessel (see Materials and methods). Notably, ozone levels in the ASITs were consistently lower than those in the flushing air, indicating further chemical reactions within the ASITs headspace or wall losses.

https://doi.org/10.5194/egusphere-2026-1720
Preprint. Discussion started: 8 April 2026

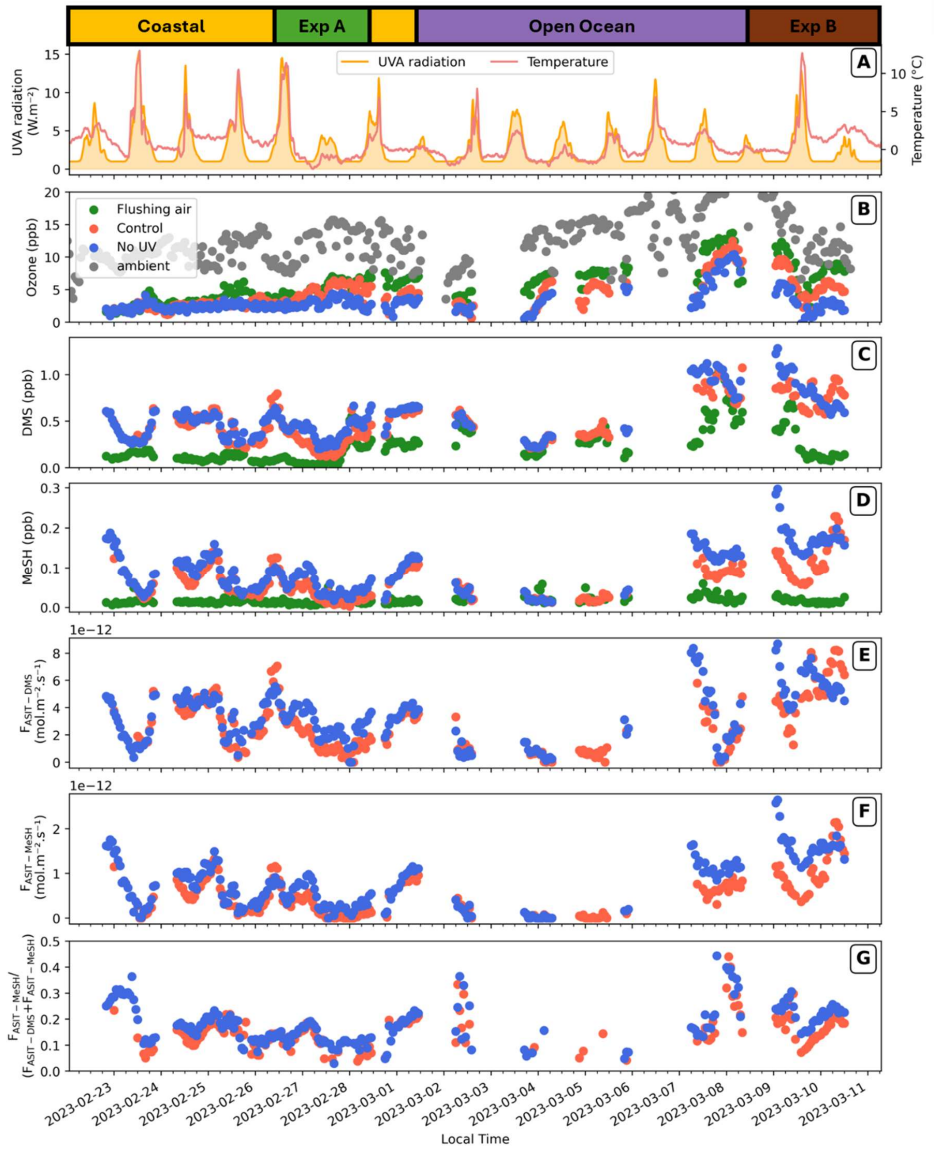

Figure 3: Time series of gaseous concentrations and sea–air fluxes of DMS and MeSH, and the $F_{ASIT\text{-}MeSH}/(F_{ASIT\text{-}DMS}+F_{ASIT\text{-}MeSH})$ ratio within the ASITs over the cruise. Dates are noted in the x axis at the bottom of the figure, and the measurement phases of the cruise are indicated at the top. A) Solar UVA radiation and ambient temperature. B) Ozone concentration in the ambient, flushing air, and the two ASITs outflow air. C) DMS and D) MeSH concentrations in the flush and ASIT outflow air. The sea–air fluxes of DMS and MeSH as well as their ratio in the ASITs (Control and no UV) are shown in E), F) and G), respectively. Symbols in B to G, as in legend inside B.

ASIT DMS and MeSH concentrations and sea–air fluxes exhibited substantial variability over the cruise (Fig. 3). For the Control-ASIT (effect of UV filtering will be discussed section 3.3) (Fig. 3.E, red markers), the $F_{ASIT\text{-}DMS}$ was on average 3.03 pmol·m^{-2}·s^{-1} (i.e., 0.26 µmol·m^{-2}·d^{-1}), peaking at 8.68 pmol·m^{-2}·s^{-1} on March 10th, while the average $F_{ASIT\text{-}MeSH}$ was 0.64 pmol·m^{-2}·s^{-1} (i.e., 0.06 µmol·m^{-2}·d^{-1}), with a maximum of 2.65 pmol·m^{-2}·s^{-1} coinciding with that of $F_{ASIT\text{-}DMS}$. Note that fluxes of both compounds were always positive, i.e., these species

https://doi.org/10.5194/egusphere-2026-1720
Preprint. Discussion started: 8 April 2026

were always degassing from seawater. Corresponding average seawater concentrations (Fig. S.2.) estimated for DMS (DMS_w) was 1.8 nM, reaching a maximum of 4.5 nM, while estimated $MeSH_w$ averaged 0.8 nM, with a peak of 3.2 nM in the Control-ASIT (Fig. S.2.).

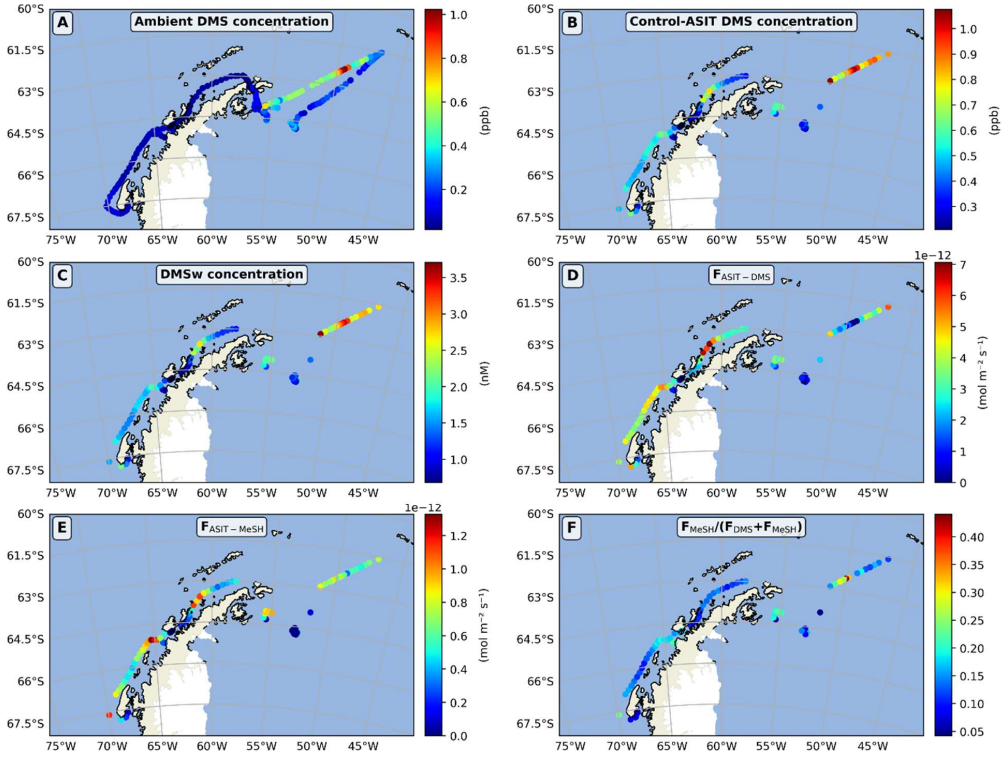

Figure 4: Ambient air DMS concentration (A) compared to ASIT air DMS concentration (B), estimated aqueous DMS concentration (C), DMS sea–air flux (D), MeSH sea–air flux (E), and the ratio of MeSH flux to DMS plus MeSH fluxes (F) in the Control–ASIT over the cruise.

The spatial variability of gaseous DMS concentrations, estimated aqueous concentrations and sea–air fluxes in the Control-ASIT are shown in Figure 4. As expected, aqueous DMS concentrations showed the same spatial variability as the gaseous DMS concentrations, with maxima measured in the open Southern Ocean north of the Antarctic Peninsula (2.5-3 nM) and minima in the Marginal Ice Zone (MIZ) (1 nM) as well as in the Gerlache Strait (< 1nM) (location indicated in Fig. 1), which was characterized by lower salinity, reflecting the inflow of fresh water from melting ice. This low salinity trend in the Gerlache Strait was confirmed twice during the ship's outward and return passages through this area. Aqueous DMS concentrations along the west coast of the Antarctic Peninsula (2.5-3 nM) were moderate (around 1.5-2 nM). Ambient air DMS concentrations (Fig. 4A) were also higher in one open-ocean transect north of the Weddell Sea (0.4-1 ppb) than over most of the rest of the cruise track (<0.3 ppb). Ambient air concentrations are a function of local fluxes from the ocean, but are also contributed by emissions upwind; so, matching observed atmospheric concentrations and emission fluxes is not straightforward. In addition to seawater concentrations, sea–air fluxes in the ASITs are, by definition, a function of incoming ambient air DMS concentrations; therefore, they showed a pattern which is different from that of estimated aqueous DMS concentrations. Fluxes can be low despite high seawater concentrations when incoming gaseous concentrations in the flushing air are high, as occurred over a portion of the transect north of the Weddell Sea. Conversely, fluxes were particularly high in coastal waters to the west of the peninsula, where DMS concentrations in the ambient air were particularly low. Air concentrations, estimated aqueous concentrations and sea–air fluxes of MeSH in the ASIT showed patterns parallel to those of DMS. The ratio of MeSH flux to the sum

https://doi.org/10.5194/egusphere-2026-1720
Preprint. Discussion started: 8 April 2026

of sulfur compound fluxes varied from 0.1 to 0.2 for most of the data (Fig. 4F and 6A). Causes of this variability will be further addressed in the following sections.

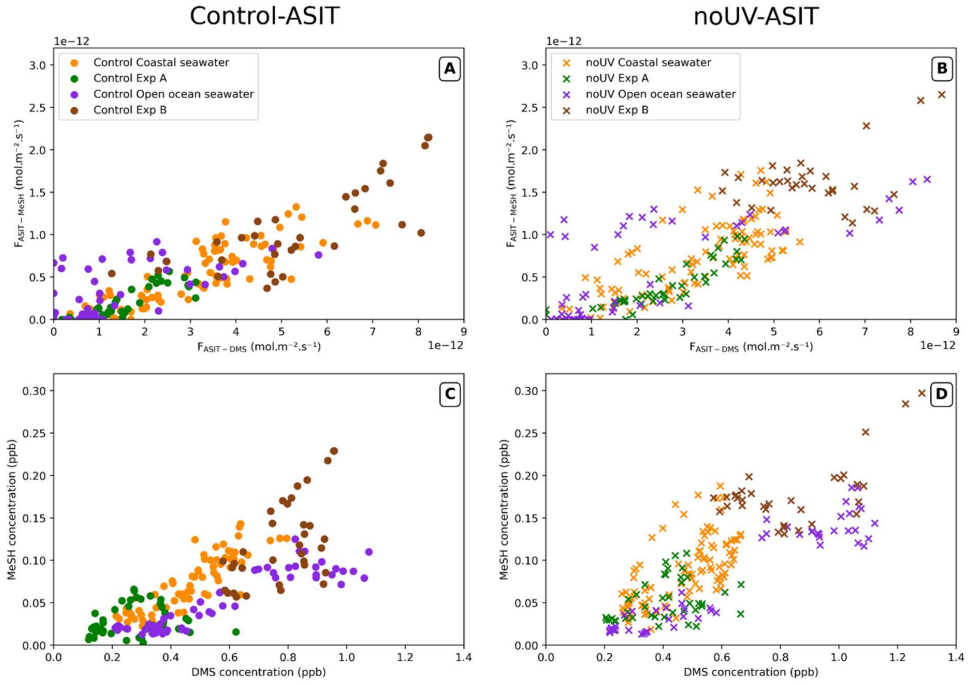

Figure 5: Relationship between hourly averaged DMS and MeSH sea–air fluxes (A, B) and air concentrations (C, D) in the Control (lefthand plots) and no-UV (righthand plots) ASIT. Colour indicates measurement periods in the coastal and open ocean.

A strong correlation was observed between sea–air MeSH and DMS fluxes in both ASITs, with R^2 values of 0.88 for the Control-ASIT and 0.81 for the noUV-ASIT, across all coastal and open ocean measurement periods (Figs. 5A and B). The median value of the $F_{ASIT-MeSH}/(F_{ASIT-DMS}+F_{ASIT-MeSH})$ ratio obtained for all data combined was 0.17 (first quartile Q1 = 0.13; third quartile Q3 = 0.22) in the Control-ASIT (Fig. 6A). There do not appear to be major differences between the enclosed experiment periods and the periods with continuous water flow into the tanks, except that the ratio was less variable during the experiments, reflecting the more stable water composition in the ASITs. However, with all measurement periods together, the average $F_{ASIT-MeSH}/(F_{ASIT-DMS}+F_{ASIT-MeSH})$ in open ocean waters was slightly higher than in coastal water types in Control-ASIT and slightly lower in noUV-ASIT.

https://doi.org/10.5194/egusphere-2026-1720
Preprint. Discussion started: 8 April 2026

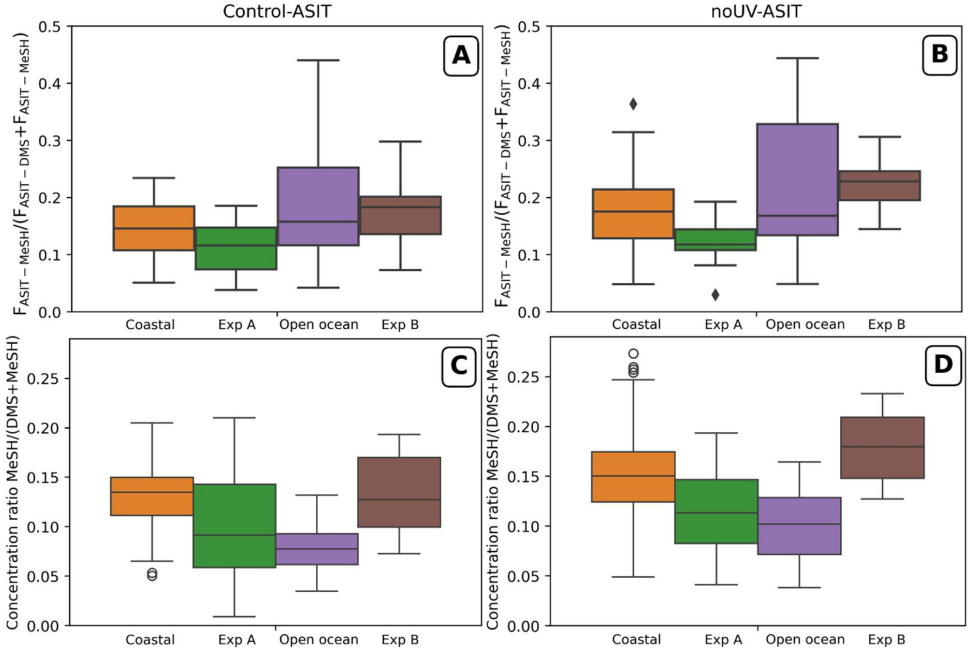

Figure 6: Boxplot of the $F_{ASIT\text{-}MeSH}/(F_{ASIT\text{-}DMS}+F_{ASIT\text{-}MeSH})$ ratio (A, B) and the air concentration ratio (C, D) for each observational period in the Control (lefthand plots) and no-UV (righthand plots) ASIT. Boxes represent the interquartile range (IQR, 25th–75th percentiles), horizontal lines the median, whiskers extend to 1.5× IQR, and outliers are plotted as points.

The diel variation of the DMS concentrations was not very clear; however, the concentrations of MeSH were higher at night and decreased through the day (Figs. 7 A and B). This pattern was clearer in the noUV-ASIT both during day and night. As a result, the diel pattern of the $F_{ASIT\text{-}MeSH}/(F_{ASIT\text{-}DMS}+F_{ASIT\text{-}MeSH})$ ratio paralleled that of $F_{ASIT\text{-}MeSH}$ (Fig. 7C).

https://doi.org/10.5194/egusphere-2026-1720
Preprint. Discussion started: 8 April 2026

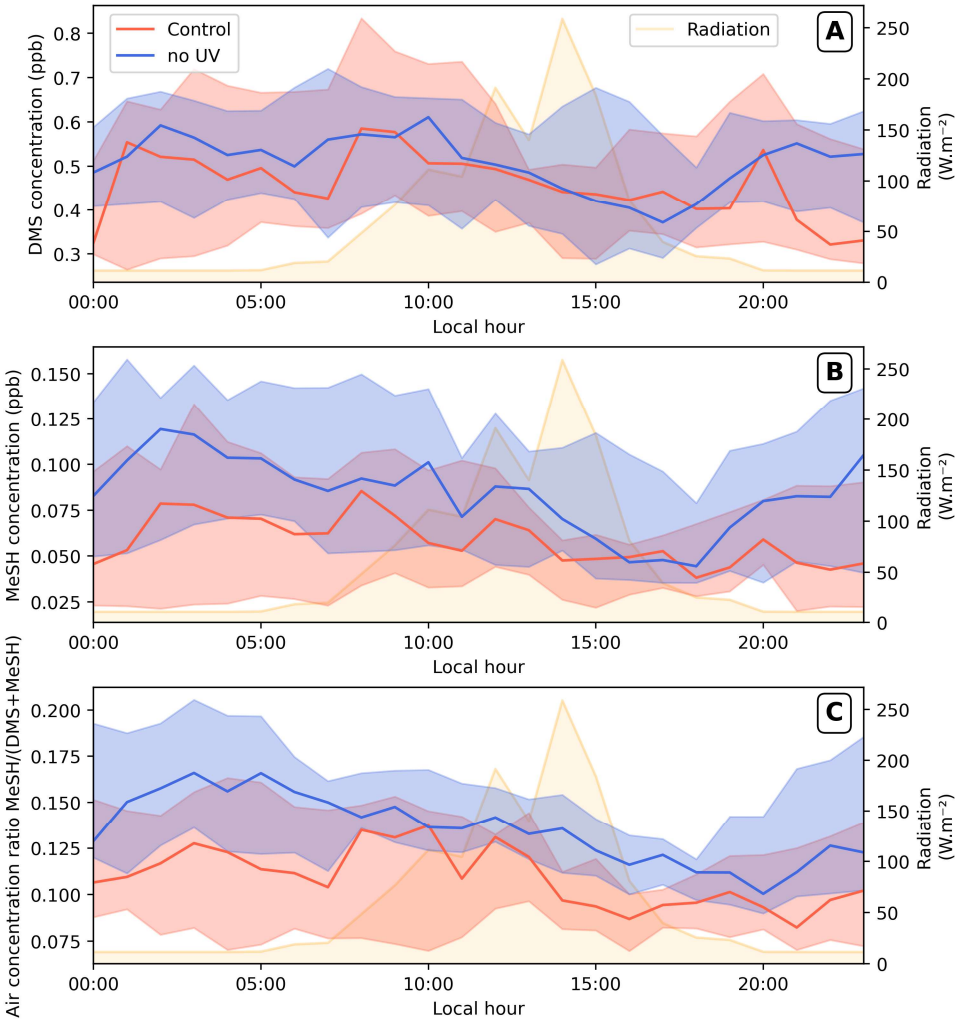

Figure 7: Median ± 1st and 3rd quartiles of the diel pattern of the gaseous DMS (A) and MeSH (B) concentrations and their ratio (C) in both ASITs (Control, red; noUV, blue) considering all data over the entire cruise (i.e. from the measurement periods, including coastal, open ocean and Experiments A and B). Irradiation daily variation is indicated by the yellow area.

3.2 New particle formation

https://doi.org/10.5194/egusphere-2026-1720
Preprint. Discussion started: 8 April 2026

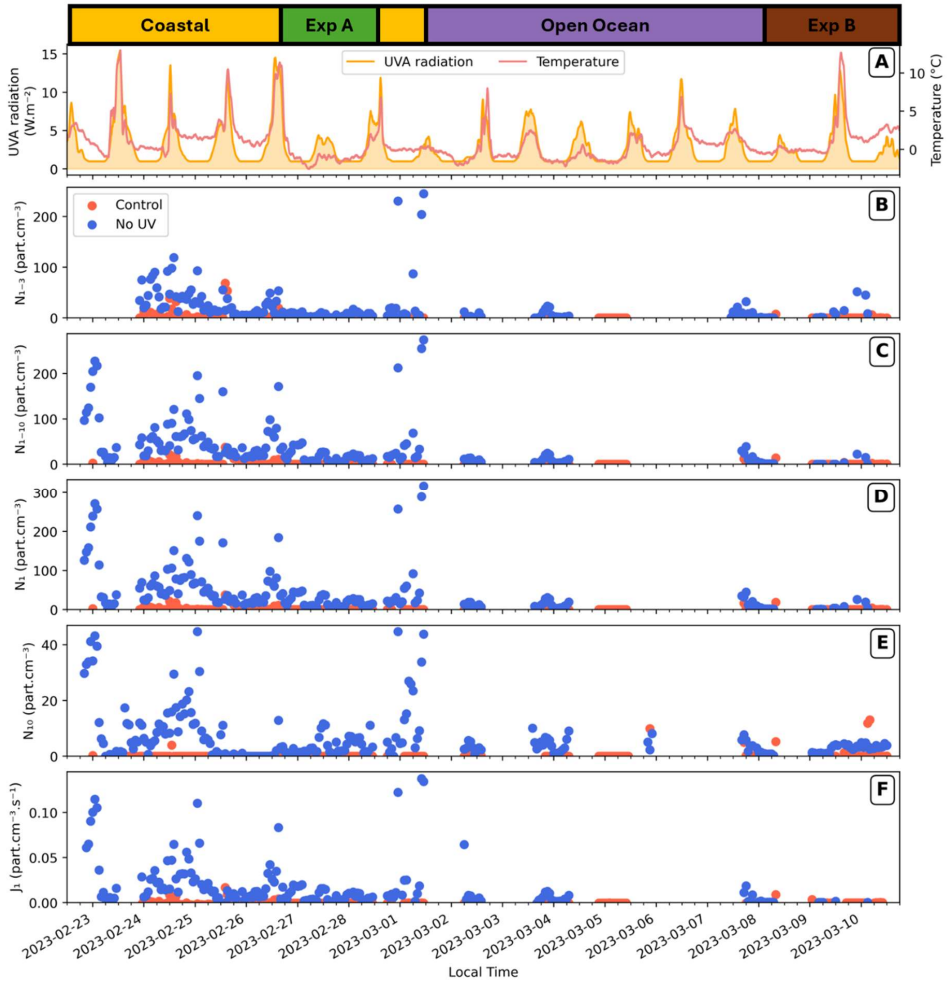

345 **Figure 8: Time series of sized particle concentrations (B-E) and particle formation rates (F) in the ASITs. Air temperature inside the ASITs and solar radiation (UVA) are indicated (A) and measurements periods are presented on top of the figure.**

The concentrations of 1-3 nm ($N_{1\text{-}3}$), 1-10 nm ($N_{1\text{-}10}$), > 1 nm (N_1) and >10 nm (N_{10}) particles are presented in Fig. 8. The formation rates of 1 nm particles (J1) are obtained using the method presented in Sect. 2. In the Control-ASIT, very few and weak new particle formation events were observed (Fig. 8) with N_1 particle concentrations reaching up to 38 particles·cm^{-3}, mainly composed of 1 to 3 nm particles, and formation rates peaked at 0.02 particles·cm^{-3}·s^{-1}. Few of these particles reached higher size than 10 nm which is consistent with the short residence time (40 mins) in the ASITs. Most of the particles in the Control-ASIT were formed with coastal waters and new particles formation occurs only in the middle of the day, around maximum radiations periods (Fig. 9). The effect of filtering UV light on new particle formation will be addressed in the next section.

https://doi.org/10.5194/egusphere-2026-1720
Preprint. Discussion started: 8 April 2026

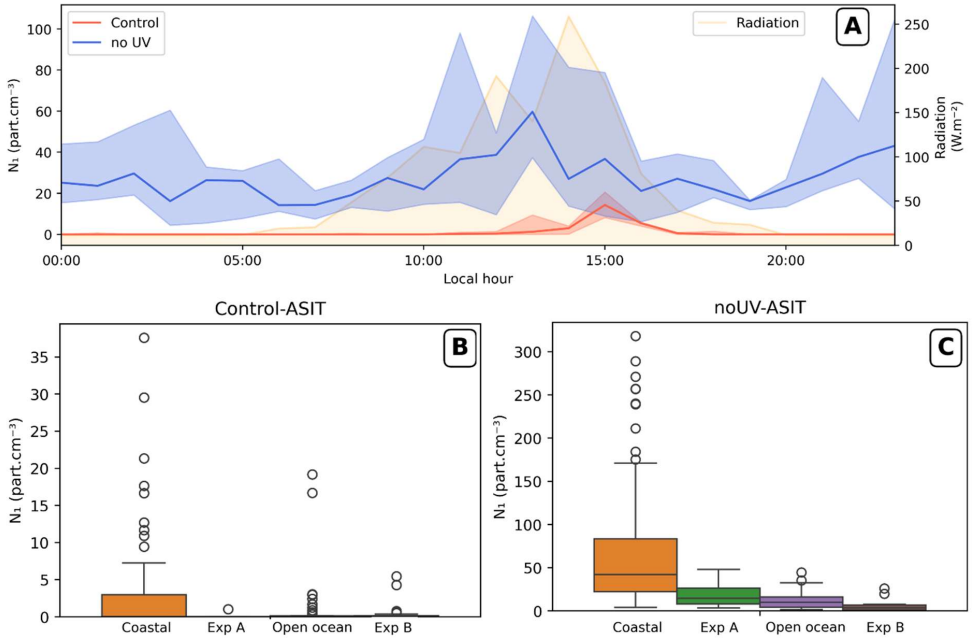

Figure 9: (A) Median diel profile of the N_1 particle concentration in the ASITs headspaces, all measurement periods merged (median ± 1st and 3rd quartile); irradiation daily variation is indicated by the yellow area. Boxplots of the N_1 particle concentration by seawater type within each ASIT headspace (B, Control; C, noUV).

3.3 Differences induced by UV

3.3.1 DMS, MeSH and ozone concentrations

Sea–air fluxes and concentrations of DMS and MeSH were consistently higher in the noUV-ASIT than in the Control-ASIT (Figs. 3C, 3D, 7A, 7B). On average, DMS fluxes were 24% higher and MeSH fluxes 58% higher in the noUV-ASIT. The difference between ASITs is statistically significant (confirmed by a paired Wilcoxon signed-rank test) both for DMS ($W = 4129$, p-value $= 1.66 \times 10^{-11}$, $r = 0.56$) and MeSH ($W = 1698$, $p = 6.12 \times 10^{-23}$, $r = 0.82$) indicating a clear negative impact of UV-light especially on MeSH concentrations (Fig. 7). These differences were even more pronounced during Experiment A and the beginning of Experiment B (Fig. 3). Decreased MeSH concentrations in the presence of UV-light were observed during the experiments and also outside the experimental periods, while for DMS, the difference between the noUV-ASIT and Control-ASIT was noticeable mostly during experiments as for the sea-air fluxes (Fig. S3). Interestingly, the highest impact of UV, especially on MeSH concentrations, occurred in the night with increased concentrations when UV light was filtered out (Fig. 7B). This effect is also observed on DMS concentrations (Fig. 7A).

The median value of the $F_{ASIT\text{-}MeSH}/(F_{ASIT\text{-}DMS}+F_{ASIT\text{-}MeSH})$ ratio obtained for all data combined was slightly lower in the Control-ASIT (Median = 0.15; Q1 = 0.11; Q3 = 0.19) than in the noUV-ASIT (Median = 0.17; Q1 = 0.13; Q3 = 0.22). This was also observed for the air concentrations ratios and calculated aqueous concentrations ratios with median values of aqueous concentrations of 0.27 (Q1 = 0.20; Q3 = 0.33) in the Control-ASIT and 0.32 (Q1 = 0.26; Q3 = 0.38) in the noUV-ASIT. Moreover, as illustrated in Figure 7C, the decrease in the ratio of MeSH to DMS linked to UV light exposure was more pronounced. Finally, the MeSH–DMS relationship was more linear in the Control-ASIT and more scattered in the noUV-ASIT, both across and within different measurements periods (Fig. 5).

https://doi.org/10.5194/egusphere-2026-1720
Preprint. Discussion started: 8 April 2026

Outside the experimental periods, ozone levels differed only slightly between the two ASITs (Fig. 3B). In contrast, during Experiments A and B, clear differences emerged in the ASIT ozone concentrations. During Experiment A, the noUV-ASIT exhibited 37% lower ozone concentrations than the Control-ASIT, and during Experiment B this difference increased to 53%.

3.3.2 Aerosol particle concentrations and formation rates

Filtering out UV light had a large impact on the formation of new particles, which were observed in significantly higher concentrations in the absence of UV-light (Fig. 8). N_1 particle concentrations reached up to 300 particles·cm^{-3} in the noUV-ASIT, and J1 highest nucleation rates were close to 0.15 particles cm^{-3}·s^{-1} (Fig. 8D, F, respectively). The highest particle concentrations were obtained with coastal waters (Fig. 9B) on both coastal sides of the Antarctic Peninsula (Fig. S.6). In contrast, particle concentrations with open ocean waters and both experiments were lower (Fig. 8B to 8E): 48, 45 and 26 particles·cm^{-3} in the noUV-ASIT for experiment A, open ocean waters, and experiment B, respectively. Moreover, experiments A and B showed lower particle concentrations than with their respective seawater outside of the experiments. Diel variations in N_1 particles (Fig. 9) showed that most new particle formation in the noUV-ASIT occurred in the middle of the day or at night, with a decrease in formation rates at the beginning and end of the daylight period. Again, these diurnal variations of N_1 differ from previous observations performed in the ASITs in the Southwestern Pacific Ocean during the Sea2Cloud ship campaign, where N_1 were preferentially formed at the end of the night prior to dawn (Chamba et al., 2023).

3.3.3 Seawater microorganisms

In Experiments A and B, in general, the abundances of most phytoplankton groups remained stable or increased, suggesting that they performed relatively well in the ASITs over the 48-hour duration of the experiments (Figs. 10 and S.5). Trends in chlorophyll-*a* concentration, a proxy for the biomass of photosynthetic organisms, corroborates this finding, remaining stable during Experiment A and increasing during Experiment B (Figs. S.4A, B). However, the different groups exhibited differing responses. The cell abundances of the biggest (15-20 µm SED nanophytoplankton, Figs. 10A, B) and smallest (<2 µm SED, picoplankton, Figs. 10G, H) size fractions were higher in Experiment A (with incubated coastal seawater), while the 7-15 µm and 2-7µm SED nanophytoplankton abundance (Figs. 10C, D, E and F) were similar or increased in some treatments during Experiment B (with open ocean water).Regarding the sensitivity to UV light, some phytoplankton were negatively impacted, especially the 7-15 µm and 2-7µm nanophytoplankton from open ocean waters in Experiment B (Figs. 10D, F). UV light had a stronger negative impact on the small sizes (2–7 µm) between 12 and 24 hours after the start of the experiment, while larger sizes (7–20 µm) exhibited more sensitivity in the 24 h to 48 h period. In contrast, only cryptophytes experienced an apparent positive response to the UV light towards the end of the experiments (Fig. S.5).

https://doi.org/10.5194/egusphere-2026-1720
Preprint. Discussion started: 8 April 2026

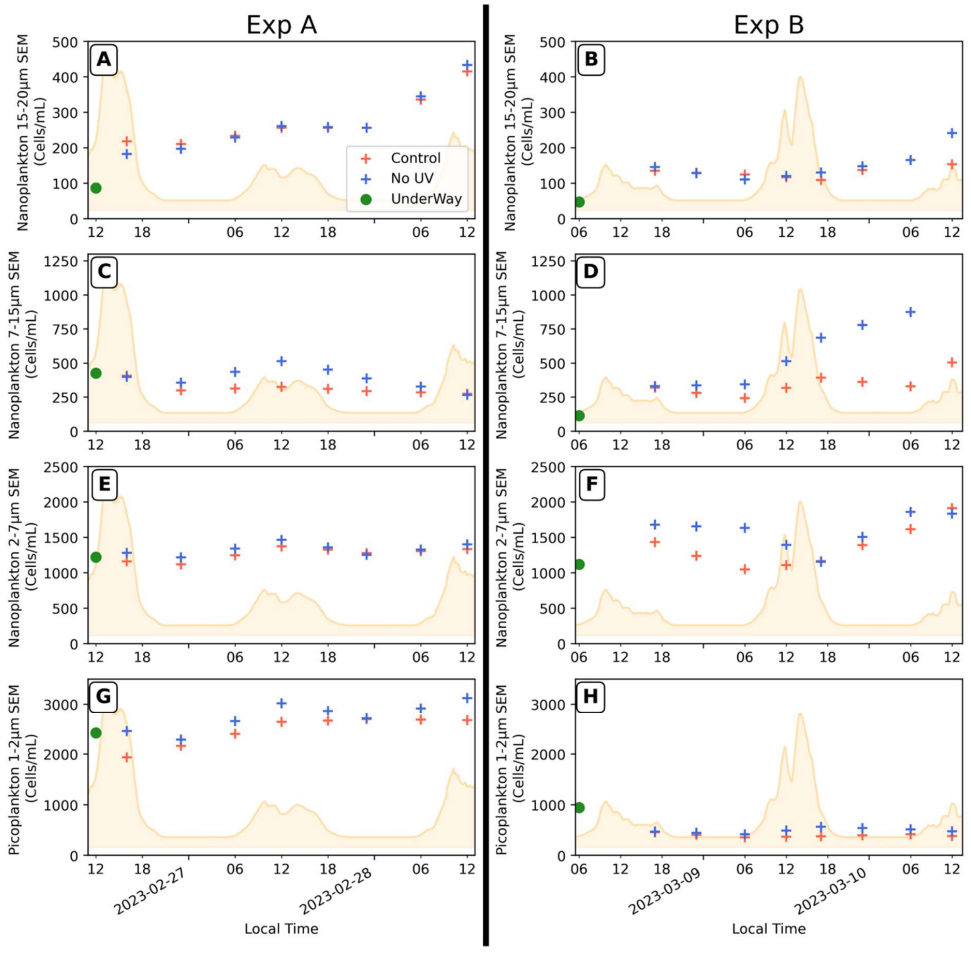

Figure 10: Evolutions of the 15-20µm SED nanophytoplankton (A, B), 7-15 µm SED (C, D), 2-7µm SED (E, F) and picoplankton 1-2 µm SED (G, H) abundances in both ASITs during Experiments A and B. The starting point (green filled circle) represents the measurement in the seawater sample from the underway inlet system at the beginning of the experiments and may not exactly reflect the initial water composition inside the ASITs. Irradiation daily variation is indicated by the yellow area.

The Fv/Fm ratio, a proxy of phytoplankton photosynthetic efficiency, showed a clear diel pattern, with lower median values during the day and higher values at night (Fig. 11). This pattern was consistent between the two ASITs and reflected the same diel variation observed in the seawater from the underway inlet measurements. However, Fv/Fm values within the ASITs exhibited less variability throughout the day and were overall higher compared to the seawater from the underway system outlet, particularly around noon. Therefore, higher photosynthetic efficiencies suggest a reduction in phytoplankton stress within the ASITs, especially at noon.

UV exposure seemed to impact phytoplankton photosynthetic efficiency as both Experiments A and B progressed, leading to lower Fv/Fm in the Control-ASIT by the end of the experiment period (Fig. S.4G, H). UV light showed little impact on the bacterial concentrations except on the second day of Experiment B (Fig. S.4F), where during a 12-hour period UV impacted negatively on the low-DNA bacteria and positively on the HNA bacteria concentrations (Fig. S.4D).

https://doi.org/10.5194/egusphere-2026-1720
Preprint. Discussion started: 8 April 2026

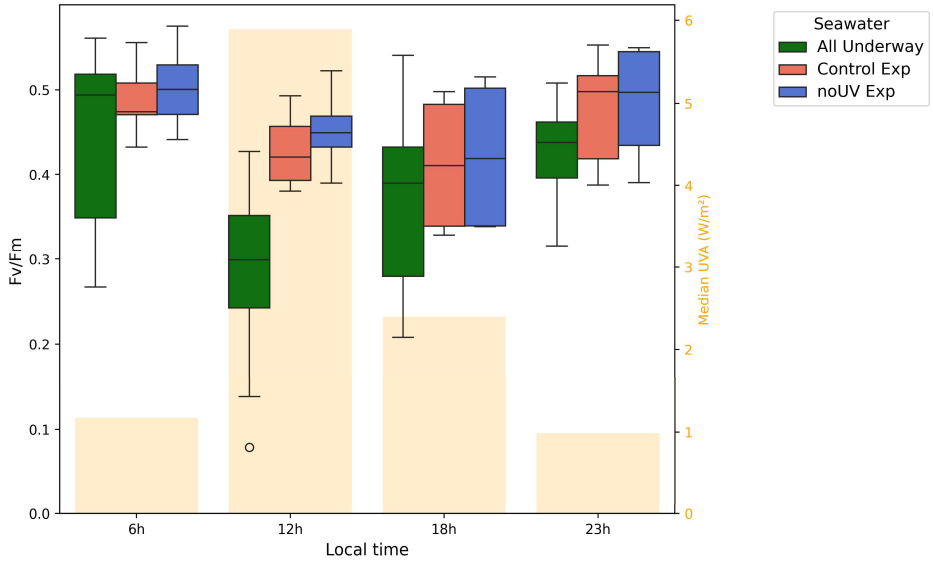

Figure 11: Diel Fv/Fm variation in samples concurrently collected from the two ASITs during both experiments (Control exp and noUV exp) and from the underway water inlet during the whole POLAR-CHANGE campaign (All Underway). Median UVA radiation is indicated by yellow bars.

4 Discussion

4.1 Gas-phase emissions and reactivity

DMS and MeSH positive sea–air fluxes indicate emission from seawater linked to marine biological processes (Fig. 3). The equivalent wind speed inside the ASIT headspace was estimated as 2–3 $m \cdot s^{-1}$ (Rocco et al., 2025a), i.e., significantly lower than typical conditions at the ocean surface. Consequently, a comparison to ambient fluxes in the literature is irrelevant but a comparison to similar experiments performed in the Southwestern Pacific Ocean during the Sea2Cloud voyage can be done (Sellegri et al. 2023). In Sea2Cloud, the average DMS fluxes in the Control-ASIT were 23.2, 8.2, and 2.9 $pmol \cdot m^{-2} \cdot s^{-1}$ (i.e. 2.0, 0.7 and 0.3 $\mu mol \cdot m^{-2} \cdot d^{-1}$) for frontal, subantarctic, and subtropical waters, respectively. The fluxes observed during POLAR-CHANGE (3.03 $pmol \cdot m^{-2} \cdot s^{-1}$, peaking at 8.68 $pmol \cdot m^{-2} \cdot s^{-1}$) were similar to Sea2Cloud fluxes in subantarctic and subtropical waters. Consequently, calculated aqueous DMS concentrations (0.3–4 nM and 1–4.3 nM for Control and noUV ASITs respectively) were similar to those measured during the Sea2Cloud in subantarctic seawaters (3–5 nM; Rocco et al., 2025a).

During Experiments A and B, the estimated lower concentrations of DMS_w in the Control-ASIT (Fig. S.2) are likely due to an aqueous-phase reactivity (loss) of DMS, which is accumulating over several days on static flow mode (Salignat et al., in review) as opposed to the continuous flow mode. Indeed, the gas-phase photochemical loss of DMS was shown to be negligible within the 40 minutes residence time of our experimental set-up (Rocco et al., 2025a, Salignat et al., in review). Salignat et al. (in review) also report that the diel profile observed for DMS in the ASIT incubated seawater during Sea2Cloud, with maxima during the night and minima during the day was explained by aqueous-phase ozonolysis when a constant (day and night) production was prescribed. Earlier, Brimblecombe and Shooter (1986) demonstrated the photooxidation of DMS in seawater under UV irradiation. Various studies have reported that photochemical degradation can account for 7% to 40% of dissolved DMS loss in the ocean (Galí et al., 2023), depending on regional conditions, and have linked these losses to oxidants produced by chromophoric dissolved organic matter (CDOM) and NO_3^- photolysis when NO_3^- concentrations are higher than 1 µM, as is the case in Antarctic waters (Bouillon and Miller, 2005). The hypothesis of aqueous-phase oxidation also provides a plausible explanation for the persistence of emission differences at night, when UV radiation is absent. Although the average residence time of the water in the ASITs was approximately six hours, the residence time in a continuously stirred reactor is a distribution of residence times

https://doi.org/10.5194/egusphere-2026-1720
Preprint. Discussion started: 8 April 2026

with some parcels being expelled from the reactor before the six hours and some parcels having much longer residence time. This means that daytime chemical transformations in the water produce compounds that persist during nocturnal periods. Additionally, ozone-mediated oxidation of DMS in seawater, as discussed by Hoffmann et al. (2016) and Salignat et al. (in review), could contribute to the observed differences between the ASITs. Since ozone concentrations were generally higher in the Control-ASIT for most of the campaign, and the ozone differential between ASITs showed a weak anti-correlation with the differences in DMS and MeSH fluxes, this mechanism may play a role. Although aqueous oxidation of MeSH could also be enhanced under these conditions, this process remains poorly characterized in the literature.

A strong positive correlation was found in DMS and MeSH fluxes (Fig. 5), as also previously reported in ASIT measurements by Rocco et al. (2025a) (R^2=0.81 in the Control-ASIT), and earlier by Novak et al. (2022) over non-enclosed coastal waters (R^2=0.65). The literature, mainly recent, reports ratios of MeSH to total volatile methylated sulfur pools and fluxes close to those reported here, generally between 0.10 and 0.40. Gros et al. (2023) reported a ratio of MeSH/(DMS+MeSH) concentrations in water averaging 0.20 in the North Atlantic, but varying greatly with latitude and regularly reaching 0.40 above 70°N. Leck and Rodhe (1991) estimated the average ratio of MeSH/(sulfur species) in the Baltic and North Seas at around 0.07, based on concentrations in water and including CS_2 and dimethyl disulfide (DMDS) among the sulfur species. Lawson et al. (2020) calculated flux ratios of 0.14 to 0.24 in the Southwest Pacific, neglecting oxidative losses at night. A ratio value of 0.16 in dissolved concentration and 0.17 in fluxes was found by Kettle et al. (2001) in the South and North Atlantic. Finally, during the Sea2Cloud campaign, the $F_{ASIT\text{-}MeSH}/(F_{ASIT\text{-}DMS}+F_{ASIT\text{-}MeSH})$ ratio ranged between 0.11 and 0.18 in the Control-ASIT (Rocco et al., 2025a). Thus, the values obtained in the present study are consistent with previous measurements, with values mainly between 0.10 and 0.20, but reaching 0.30 to 0.45 mostly in open ocean waters. Air concentration ratio within the Control-ASIT headspace (median of 0.11; Q1 = 0.8; Q3 = 0.14) were in the range of those reported by Mynard et al. (2025), between their Antarctic Ice-Edge (median of 0.07) and the subtropical front region (0.11-0.15).

The diel pattern of MeSH concentrations showed a decrease in the afternoon, in both ASITs, that may mainly be resulting from the higher gas-phase OH-reactivity (or photochemical loss) of MeSH compared to DMS, within the 40 min residence time in the ASIT's headspace. Greater chemical loss for MeSH than for DMS would then be behind the observed diel variation of the air MeSH/(MeSH+DMS) concentration ratio, as also suggested by Mynard et al. (2025), and could explain the significant differences in MeSH concentration between the two ASITs and a lower MeSH/(MeSH+DMS) ratio during the day compared to night, even outside the experimental periods. These observations closely resemble the diel pattern reported by Novak et al. (2022). Lawson et al. (2020) reported broadly similar diel profiles for DMS and MeSH, with a production minimum around 4 p.m. (local time) for both compounds, a trend most evident for MeSH in our experiments. However, a closer look at our measurements reveals that the MeSH concentration differs from one ASIT to the other most at night, which points to the oxidation of MeSH in the Control-ASIT being from another oxidant than OH (i.e., a nighttime aqueous-phase oxidant at larger concentrations in the presence of daytime UV), or to an impact of UV on the biology processes leading to a change in the production of MeSH in the seawater at night.

The difference in ozone concentration between ASITs may be attributed to several factors, including chemical reactions with other gaseous species, interfacial reactions during the air residence time (~40 minutes), or aqueous-phase reactions occurring over the 6-hour water residence time. These ozone losses, which occasionally reached 100% between the flushing air and ASIT headspace, were variable over time, suggesting that chemical reactivity, rather than physical deposition alone, played a significant role. If physical losses to surfaces were dominant, they would likely remain relatively constant or vary in relation to temperature. The noUV-ASIT lid blocked nearly all radiation below 375 nm (Fig. S.1), which causes most photochemical processes. In the presence of NO, the photolysis of NO_2 and NO_3 (which requires wavelengths <410 nm; Bower et al., 1993; Andersen et al., 2022) would be inhibited, potentially leading to a reduction in ozone production while ozone consumption continues unabated. One other potential explanation for the increased ozone losses in the noUV-ASIT is a higher ozone consumption, that could be due to enhanced water-to-air net fluxes of reactive compounds, particularly DMS and MeSH, whose fluxes were indeed higher in the noUV-ASIT during both experiments (see Fig. 3). It could also be the ozonolysis of organic matter, accumulated over time especially during experiments, potentially leading to

https://doi.org/10.5194/egusphere-2026-1720
Preprint. Discussion started: 8 April 2026

more VOC emissions (Kilgour et al., 2024). The increased difference between ASITs in Experiments A and B suggests that UV removal had a significant impact on the aqueous-phase chemistry (as discussed earlier) that in turn impacts ozone losses to the aqueous phase during experiments. The temporal pattern of these changes also provides insight into the relevant timescales: the differences between the two ASITs emerged within the first 12 hours of the experiments, reaching 37% higher ozone in the Control-ASIT compared to noUV-ASIT in Experiment A and 38% in Experiment B at that time point. This indicates that reactions in the aqueous phase and associated emission processes occur over timescales longer than six hours, but less than 12 hours in this experimental setup.

4.2 Links between dissolved gases and microorganisms during experiments

In Experiment A, which involved incubating coastal water in the ASITs for two days, DMS and MeSH seawater concentrations slightly decreased over time, particularly in the Control-ASIT, where MeSH concentrations became almost zero, before rising up again (Fig. S.5). In experiment B, which was similar to experiment A but with a different phytoplankton composition from open ocean waters, concentrations were higher, and the difference between the two ASITs was greater than in Experiment A, with MeSH concentrations initially 50% higher in the noUV-ASIT than in the Control-ASIT. As Experiment B progressed, the differences in DMS and MeSH concentrations between the two ASITs diminished, until a point where concentrations were even higher in the Control-ASIT.

Among measured microorganisms, cryptophytes, a sub-group of the nanophytoplankton, were the ones whose abundance variability most resembled the estimated aqueous concentrations of the sulfur compounds in both experiments and in both ASITs (Fig. S.5). In Experiment A, the covariation between cryptophytes and DMS concentration in the Control-ASIT was significant, with a gradual drop in the first 36 hours followed by a concomitant increase. Moreover, during Experiment B, cryptophytes were the only phytoplankton group whose concentration, initially lower, became higher in the Control-ASIT than in the noUV-ASIT from 09 March at noon on. This was followed by DMS concentrations in the Control-ASIT reaching and even exceeding those in the noUV-ASIT, followed shortly by an increase in MeSH concentrations. These observations suggest a connection between cryptophytes and the MeSH and DMS production mechanisms. The co-variation of MeSH and DMS concentrations with cryptophyte abundance during the experiments is consistent with the role of this taxonomic group as high DMSP producers in Antarctic waters (McParland and Levine, 2019). This does not exclude however, that other protists groups (i.e. diatoms, dinoflagellates, etc.) could play also a role in different seasonal periods of the Antarctic ecosystem.

The diel profile of Fv/Fm, typically observed in the surface ocean, where diurnal exposure to high light (including UV) leads to some degree of stress on the photosynthetic machinery, showed differences between the Control-ASIT and the noUV-ASIT and therefore could partially explain differences in production of MeSH during the experiments. Notably, during enclosed-water experiments, a diurnal increase in HNA bacterial abundance coincided with a severe decrease in phytoplankton's photosynthetic efficiency (Fv/Fm), and both were more acute in the presence of UV. It can be speculated that solar radiation stress in phytoplankton cells results in the release of organic compounds, including DMSP, that would have fostered bacterial growth as reflected in the increase of (active) HNA bacteria. In turns, this could have led to higher gross MeSH production by bacterial DMSP catabolism. The fact that air MeSH concentrations in the ASITs were higher during the night and higher in the noUV-ASIT points to aqueous, solar radiation dependent losses overcoming potential increases in gross MeSH production.

A significant positive relationship between estimated aqueous concentrations of MeSH and DMS and HNA bacterial abundances was also observed in both ASITs (R^2 = 0.43 and 0.49 in Control-ASIT; R^2 = 0.57 and 0.63 for noUV-ASIT, respectively for MeSH and DMS). This relationship was particularly noticeable in open ocean waters (Fig. 12). A relationship of sulfur compounds with virus abundance was also observed in both ASITs during experiments (Fig. S.8).

https://doi.org/10.5194/egusphere-2026-1720
Preprint. Discussion started: 8 April 2026

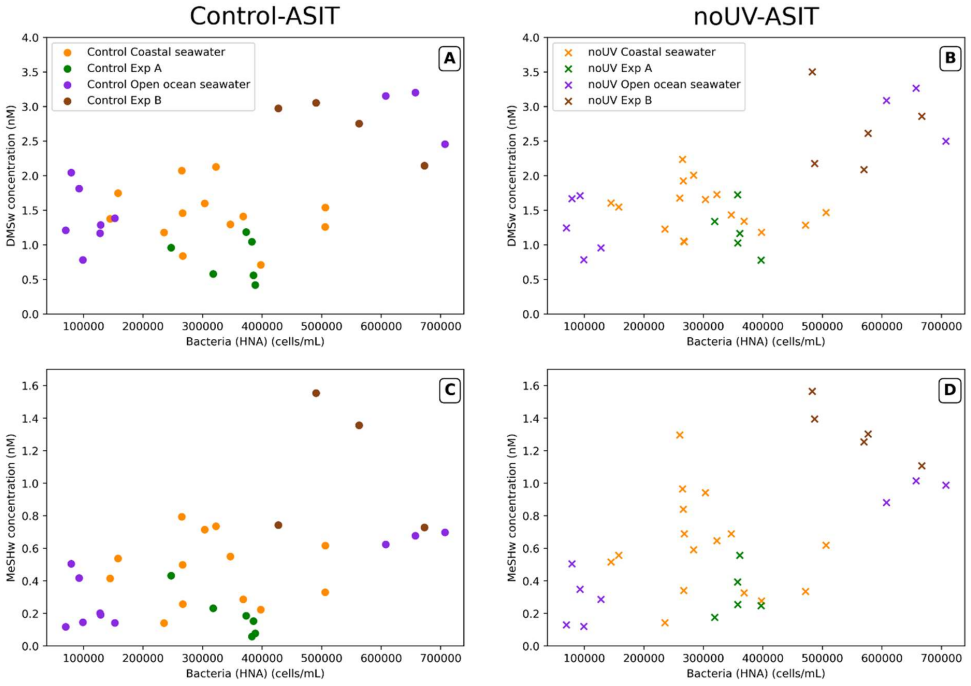

Figure 12: Scatter plots of calculated aqueous DMSw (A, B) and MeSHw (C, D) concentrations and the abundance of high-DNA bacteria. Points are coloured according to the measurement periods (see Fig. 3).

The positive relationship between bacteria and sulfur compounds had been previously observed during the Sea2Cloud campaign (Rocco et al., 2025a). This relationship has been documented in several studies and is explained by the ability of bacteria to cleave and demethylate-demethiolate DMSP, giving rise to DMS and MeSH, respectively (Kiene, 1996; Kilgour et al., 2022). The proportion of each compound in the production, as well as in the concentrations, depends on several factors, including 1) DMSP release by exudation or mortality of the algal producers, 2) whether or not the main algal DMSP producers harbor DMSP lyases and are therefore capable of releasing DMS as well, 3) the relative proportion of bacterial genes (and the corresponding enzymes) for cleavage and demethylation (which mostly depends on the taxonomic composition of the bacterial assemblage), and 4) the relative activity of these enzymes (which may depend on bacterial sulfur and carbon demands relative to DMSP availability) (Simó 2001; Sun et al., 2016; Hopkins et al., 2023).

None of the biological variables available showed a strong correlation with aqueous DMS and MeSH concentrations throughout the entire campaign when considering the continuous flow mode of our ASITs set-up, except for the open ocean period with Chl-*a*. Since cryptophytes, nanophytoplankton, and bacterial abundances showed some co-variation with these sulfur volatiles during the experiments, one explanation for this not occurring in the continuous flow mode could be that in an open system with different lifetimes and dynamics for biological and chemical components, cause-effect relationships between seawater microorganisms dissolved volatiles are harder to capture than in a closed system such as during the ASIT experiments.

https://doi.org/10.5194/egusphere-2026-1720
Preprint. Discussion started: 8 April 2026

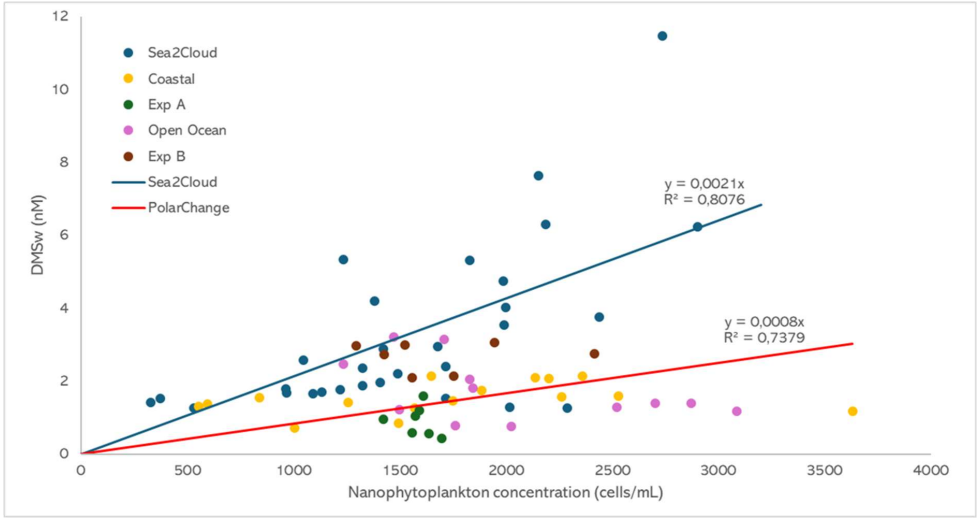

595 **Figure 13: Correlation between estimated aqueous DMS concentrations in the Control-ASIT and 2-20 µm nanophytoplankton cell abundances. The blue dots are the measurements during the Sea2Cloud cruise, the blue line shows the DMS vs nanophytoplankton concentration in that study (Rocco et al., 2025a) and the red line includes all measurements from the POLAR-CHANGE campaign.**

600 Rocco et al., (2025a) observed a positive relationship between measured DMS_w and 2-20 µm nanophytoplankton abundance during the Sea2Cloud campaign. If forced to zero, the relationship between DMS_w and nanophytoplankton from the POLAR-CHANGE data, that would be representative of ocean below 60°S, would have a slope of 0.0008 nM $cells^{-1}$ mL

605 Moreover, it must be noted that significant positive correlation was observed between DMSP, the main DMS precursor, and nanophytoplankton (particularly cryptophytes) in sea surface samples of the same cruise (Wohl et al., submitted). A similar relationship between the estimated $MeSH_w$ concentrations and 2-15 µm nanophytoplankton concentration was observed during experiments A and B (Fig. S8). All in all, in the absence of a better biological proxy for predicting seawater DMS levels, nanophytoplankton cell abundances better
610 captures DMS variability across coastal and open ocean waters than Chl-*a* concentrations.

4.3 New particle formation

The maximum particle concentrations observed during this campaign were slightly higher than those observed
615 during the previous campaign using the same ASIT setup (Chamba et al., 2023), where N_1 particles reached concentrations of 180 particles cm^{-3}, and nucleation rates were up to 0.08 particles cm^{-3} s^{-1}. The present nucleation rates in the noUV-ASIT, reaching 0.15 particles $cm^{-3} \cdot s^{-1}$, are slightly above those reported for Antarctic areas (0.05 particles $cm^{-3} \cdot s^{-1}$) and below those reported for Arctic areas in the ambient open atmosphere (0.51 particles $cm^{-3} \cdot s^{-1}$) (Kerminen, 2018).

620

https://doi.org/10.5194/egusphere-2026-1720
Preprint. Discussion started: 8 April 2026

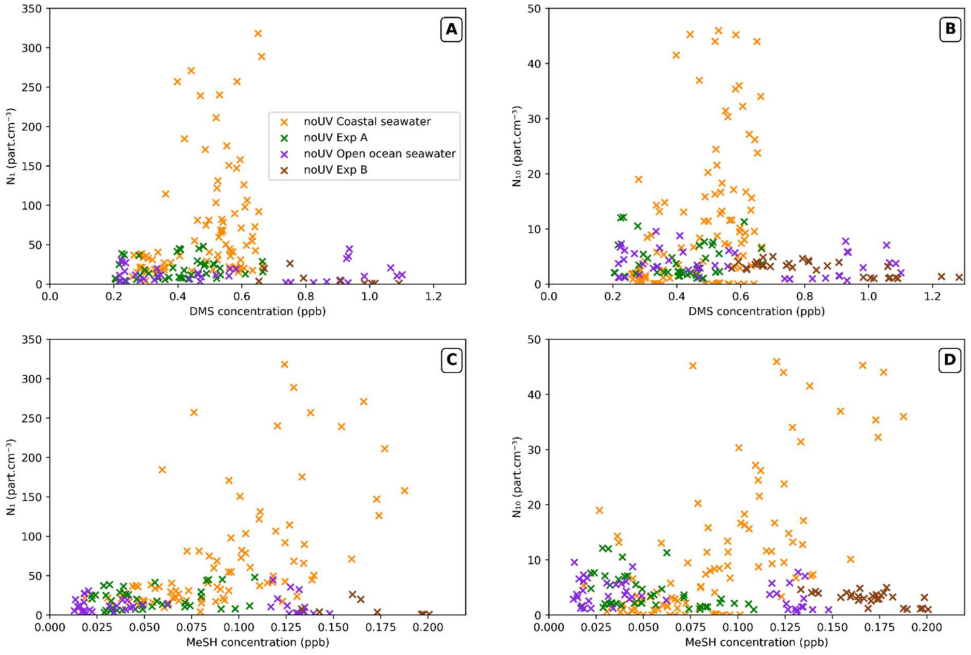

Figure 14: Scatter plots of N_1 (A, C) and N_{10} (B, D) particle concentrations and gaseous DMS (A, B) and MeSH (C, D) concentrations in the noUV-ASIT, with colour referring to the measurements period (as in Fig. 3).

Air MeSH concentrations showed the strongest positive correlation to N_1 and N_{10} particle concentrations in the noUV-ASIT in continuous flow mode with coastal waters ($R^2 = 0.56$ for N_{10}; yellow in Fig. 14). This correlation degraded in the case of DMS ($R^2 = 0.31$). No significant relationship of MeSH and DMS to particle concentrations was observed in the noUV-ASIT with open ocean waters or during Experiments A and B, nor in the Control-ASIT in any observational period when particle concentrations remained low.

It is important to note that, like during the Sea2Cloud campaign (Chamba et al., 2023), no biological variable or gaseous compound showed differences between the ASITs as pronounced as the concentrations of particles, which were up to a factor of 10 higher in the noUV-ASIT. As concluded from the Sea2Cloud study, the presence of DMS and MeSH alone did not explain the formation of new particles in the enclosures. However, a significant positive correlation was found between N_1 and the nanophytoplankton cell abundance during experiments, particularly with the 7-15µm nanophytoplankton population (Fig. S.8). This calls for further studies identifying the new particle precursors related to nanophytoplankton.

5 Conclusions

Sea–air fluxes measured inside the ASITs were always positive, i.e. degassing from seawater to air, ranging up to 8.68 pmol·m^{-2}·s^{-1} for DMS and up to 2.65 pmol·m^{-2}·s^{-1} for MeSH. DMS fluxes did not vary significantly between day and night conditions, however the $F_{ASIT\text{-}MeSH}/(F_{ASIT\text{-}DMS}+F_{ASIT\text{-}MeSH})$ ratio did have a clear maximum at night and a decrease during daytime due to diel variation in $F_{ASIT\text{-}MeSH}$. The diel pattern of the $F_{ASIT\text{-}MeSH}/(F_{ASIT\text{-}DMS}+F_{ASIT\text{-}MeSH})$ ratio could not be explained by daytime gas-phase photochemistry of MeSH compared to DMS. Estimated aqueous DMS concentrations showed maxima in the open ocean north of the Weddell Sea (2.5-3 nM) and minima in the MIZ of the Weddell Sea (1 nM) as well as in the Gerlache Strait (< 1nM). Intermediate concentrations were estimated along the western coast of the peninsula (around 1.5-2 nM). None of the biological variables available showed a strong correlation with estimated aqueous DMS and MeSH concentrations

https://doi.org/10.5194/egusphere-2026-1720
Preprint. Discussion started: 8 April 2026

throughout the entire campaign, although cryptophytes, nanophytoplankton, and notably bacterial concentrations showed some co-variation with the aqueous concentrations during the Experiments A and B. The ratio of estimated aqueous DMS concentration to nanophytoplankton cell abundance varied less than the ratio to Chl-*a* concentration across the coastal and open-ocean waters, and during Experiments A and B. Therefore, in the absence of a better biological proxy for predicting DMS concentrations, nanophytoplankton cell abundances would be a better choice than Chl-*a* concentrations.

A negative impact of UV-light on both DMS and MeSH sea–air fluxes was observed, with DMS fluxes being 24% higher and MeSH fluxes 58% higher in the noUV-ASIT compared to the Control-ASIT. Interestingly, the highest impact of filtering out UV, especially the increase of airs MeSH concentrations, was seen during the night, indicating that seawater reactivity or biology had been impacted by UV during the previous diurnal period. UV light caused a slight increase in phytoplankton stress at noon and had a negative impact on the mid-term development of nanophytoplankton, especially with open-ocean waters. Removal of UV-light increased the new particle formation within the ASIT headspace, with formation rates reaching 0.15 particles cm^{-3} s^{-1} observed with coastal waters west of the Antarctic Peninsula only in the noUV-ASIT. These nucleation rates are slightly above those reported for Antarctic areas and below those reported for Arctic areas. Newly-formed particle concentrations in the noUV-ASIT headspace were best correlated to air MeSH concentrations and to a lesser extent to DMS in run-through measurements with coastal seawaters. The presence of DMS and MeSH alone did not explain the formation of new particles in the enclosures, and no biological variable showed differences between the ASITs as pronounced as the concentrations of airborne nanoparticles, which were up to a factor of 10 higher in the enclosure with no UV light. These results call for a yet-to-identify new particle formation process that, despite being of diurnal occurrence, is enhanced by reduced UV radiation.

Data availability

ASITs, ambient air measurements and meteo data as well as position of the ship during the campaign are available for download at https://doi.org/10.5281/zenodo.19222956 (Chamba et al., 2026)

Authors contribution

KS and GC designed the experiments, MD coordinated the POLAR-CHANGE cruise; GC, KS, VG, CR, AC, J-MP and MR prepared atmospheric instrumentation; GC and KS performed ASIT's headspace measurements; QG-B and RS performed Fv:Fm measurements; AR, E-LS and YC performed flow cytometry analysis; DV performed sampling and analysis of viruses; GC performed atmospheric data analysis; KS, VG and CR discussed data analysis; GC and KS wrote the paper with contributions from RS, EB, MV, LW, DV, VG, CR and CW.

Competing interests

The authors have no competing interests to declare.

Acknowledgements

We thank Ana Sotomayor and the crew of the RV *Hesperides* for the logistic support, making possible the data collection of this study. We thank Jair Antonio Arévalo Lirio, Luz B. Ferrer and Sofía Ibáñez Homedes for assistance counting flagellates and bacteria. We also thank Angelica Bianco and Guillaume Voyard for the characterisation of the transparency of ASIT lids.

Financial support

The research received funding from the European Research Council (ERC) under the Horizon 2020 research and innovation programme (Sea2Cloud Grant Agreement 771369), endorsed by SOLAS. The POLAR-CHANGE project (Aerosol Emissions in Changing Polar Environments, PID2019-110288RB-I00) received funding from the Spanish Ministerio de Ciencia e Innovación (MICIN). Further support was provided through an Advanced Grant from the European Research Council (ERC-2018-AdG #834162). This study is part of the POLARCSIC platform activities, and had the institutional support of the 'Severo Ochoa Centre of Excellence' accreditation (CEX2019-000928-S) to the ICM-CSIC.

https://doi.org/10.5194/egusphere-2026-1720
Preprint. Discussion started: 8 April 2026

References

Andersen, S. T., Nelson, B. S., Read, K. A., Punjabi, S., Neves, L., Rowlinson, M. J., Hopkins, J., Sherwen, T., Whalley, L. K., Lee, J. D., and Carpenter, L. J.: Fundamental oxidation processes in the remote marine atmosphere investigated using the NO–NO $_2$ –O $_3$ photostationary state, Atmos. Chem. Phys., 22, 15747–15765, https://doi.org/10.5194/acp-22-15747-2022, 2022.

Andreae, M. O.: Ocean-atmosphere interactions in the global biogeochemical sulfur cycle, Marine Chemistry, 30, 1–29, https://doi.org/10.1016/0304-4203(90)90059-L, 1990.

Asher, E. C., Dacey, J. W. H., Stukel, M., Long, M. C., and Tortell, P. D.: Processes driving seasonal variability in DMS, DMSP, and DMSO concentrations and turnover in coastal Antarctic waters, Limnology & Oceanography, 62, 104–124, https://doi.org/10.1002/lno.10379, 2017.

Bates, T. S., Lamb, B. K., Guenther, A., Dignon, J., and Stoiber, R. E.: Sulfur emissions to the atmosphere from natural sourees, J Atmos Chem, 14, 315–337, https://doi.org/10.1007/BF00115242, 1992.

Biggs, T. E. G., Huisman, J., and Brussaard, C. P. D.: Viral lysis modifies seasonal phytoplankton dynamics and carbon flow in the Southern Ocean, ISME J, 15, 3615–3622, https://doi.org/10.1038/s41396-021-01033-6, 2021.
Bouillon, R.-C. and Miller, W. L.: Photodegradation of Dimethyl Sulfide (DMS) in Natural Waters: Laboratory Assessment of the Nitrate-Photolysis-Induced DMS Oxidation, Environ. Sci. Technol., 39, 9471–9477, https://doi.org/10.1021/es048022z, 2005.

Bower, J. S., Broughton, G. F. J., and Willis, P. G.: Measurements of urban photochemical oxidants, Royal Society of Chemistry, 1993.

Brimblecombe, P. and Shooter, D.: Photo-oxidation of dimethylsulphide in aqueous solution, Marine Chemistry, 19, 343–353, https://doi.org/10.1016/0304-4203(86)90055-1, 1986.

Brussaard, C. P. D.: Optimization of Procedures for Counting Viruses by Flow Cytometry, Appl Environ Microbiol, 70, 1506–1513, https://doi.org/10.1128/AEM.70.3.1506-1513.2004, 2004.

Carpenter, L. J., Archer, S. D., and Beale, R.: Ocean-atmosphere trace gas exchange, Chem. Soc. Rev., 41, 6473, https://doi.org/10.1039/c2cs35121h, 2012.

Chamba, G., Rissanen, M., Barthelmeß, T., Saiz-Lopez, A., Rose, C., Iyer, S., Saint-Macary, A., Rocco, M., Safi, K., Deppeler, S., Barr, N., Harvey, M., Engel, A., Dunne, E., Law, C. S., and Sellegri, K.: Evidence of nitrate-based nighttime atmospheric nucleation driven by marine microorganisms in the South Pacific, Proc. Natl. Acad. Sci. U.S.A., 120, e2308696120, https://doi.org/10.1073/pnas.2308696120, 2023.

Chamba, G., Gros, V., Pichon, J.-M., Aurélie, C., and Sellegri, K.: ASITs experiments data for the 2023 POLAR-CHANGE campaign, https://doi.org/10.5281/ZENODO.19222956, 2026.

Charlson, R. J., Lovelock, J. E., Andreae, M. O., and Warren, S. G.: Oceanic phytoplankton, atmospheric sulphur, cloud albedo and climate, Nature, 326, 655–661, https://doi.org/10.1038/326655a0, 1987.

Constable, A. J., Harper, S., Dawson, J., Holsman, K., Mustonen, T., Piepenburg, D., and Rost, B.: Cross-Chapter Paper 6: Polar Regions, edited by: Pörtner, H. O., Roberts, D. C., Tignor, M., Poloczanska, E. S., Mintenbeck, K., Alegría, A., Craig, M., Langsdorf, S., Löschke, S., Möller, V., Okem, A., and Rama, B., Climate Change 2022: Impacts, Adaptation and Vulnerability. Contribution of Working Group II to the Sixth Assessment Report of the Intergovernmental Panel on Climate Change, 2319–2368, https://doi.org/10.1017/9781009325844.023.2319, 2022.

https://doi.org/10.5194/egusphere-2026-1720
Preprint. Discussion started: 8 April 2026

Evans, C., Pearce, I., and Brussaard, C. P. D.: Viral-mediated lysis of microbes and carbon release in the sub-Antarctic and Polar Frontal zones of the Australian Southern Ocean, Environmental Microbiology, 11, 2924–2934, https://doi.org/10.1111/j.1462-2920.2009.02050.x, 2009.

Galí, M., Devred, E., Pérez, G. L., Kieber, D. J., and Simó, R.: Global Ocean dimethylsulfide photolysis rates quantified with a spectrally and vertically resolved model, Limnol Oceanogr Letters, 8, 760–769, https://doi.org/10.1002/lol2.10342, 2023.

Gasol, J. M. and Del Giorgio, P. A.: Using flow cytometry for counting natural planktonic bacteria and understanding the structure of planktonic bacterial communities, Sci. mar., 64, 197–224, https://doi.org/10.3989/scimar.2000.64n2197, 2000.

Gorbunov, M., Shirsin, E., Nikonova, E., Fadeev, V., and Falkowski, P.: A multi-spectral fluorescence induction and relaxation (FIRe) technique for physiological and taxonomic analysis of phytoplankton communities, Mar. Ecol. Prog. Ser., 644, 1–13, https://doi.org/10.3354/meps13358, 2020.

Gorbunov, M. Y. and Falkowski, P. G.: Using Chlorophyll Fluorescence to Determine the Fate of Photons Absorbed by Phytoplankton in the World's Oceans, Annu. Rev. Mar. Sci., 14, 213–238, https://doi.org/10.1146/annurev-marine-032621-122346, 2022.

Gros, V., Bonsang, B., Sarda-Estève, R., Nikolopoulos, A., Metfies, K., Wietz, M., and Peeken, I.: Concentrations of dissolved dimethyl sulfide (DMS), methanethiol and other trace gases in context of microbial communities from the temperate Atlantic to the Arctic Ocean, Biogeosciences, 20, 851–867, https://doi.org/10.5194/bg-20-851-2023, 2023.

Häder, D. P., Kumar, H. D., Smith, R. C., and Worrest, R. C.: Effects of solar UV radiation on aquatic ecosystems and interactions with climate change, Photochem Photobiol Sci, 6, 267–285, https://doi.org/10.1039/b700020k, 2007.

Hernando, M., Varela, D. E., Malanga, G., Almandoz, G. O., and Schloss, I. R.: Effects of climate-induced changes in temperature and salinity on phytoplankton physiology and stress responses in coastal Antarctica, Journal of Experimental Marine Biology and Ecology, 530–531, 151400, https://doi.org/10.1016/j.jembe.2020.151400, 2020.

Hoffmann, E. H., Tilgner, A., Schrödner, R., Bräuer, P., Wolke, R., and Herrmann, H.: An advanced modeling study on the impacts and atmospheric implications of multiphase dimethyl sulfide chemistry, Proc. Natl. Acad. Sci. U.S.A., 113, 11776–11781, https://doi.org/10.1073/pnas.1606320113, 2016.

Hopkins, F. E., Archer, S. D., Bell, T. G., Suntharalingam, P., and Todd, J. D.: The biogeochemistry of marine dimethylsulfide, Nat Rev Earth Environ, 4, 361–376, https://doi.org/10.1038/s43017-023-00428-7, 2023.

Jackson, R. and Gabric, A.: Climate Change Impacts on the Marine Cycling of Biogenic Sulfur: A Review, Microorganisms, 10, 1581, https://doi.org/10.3390/microorganisms10081581, 2022.

Joge, S. D., Mansour, K., Simó, R., Galí, M., Steiner, N., Saiz-Lopez, A., and Mahajan, A. S.: Climate warming increases global oceanic dimethyl sulfide emissions, Proc. Natl. Acad. Sci. U.S.A., 122, e2502077122, https://doi.org/10.1073/pnas.2502077122, 2025.

Kerminen, V.-M., Chen, X., Vakkari, V., Petäjä, T., Kulmala, M., and Bianchi, F.: Atmospheric new particle formation and growth: review of field observations, Environ. Res. Lett., 13, 103003, https://doi.org/10.1088/1748-9326/aadf3c, 2018.

https://doi.org/10.5194/egusphere-2026-1720
Preprint. Discussion started: 8 April 2026

Kettle, A. J., Rhee, T. S., Von Hobe, M., Poulton, A., Aiken, J., and Andreae, M. O.: Assessing the flux of different volatile sulfur gases from the ocean to the atmosphere, J. Geophys. Res., 106, 12193–12209, https://doi.org/10.1029/2000JD900630, 2001.

Kiene, R. P.: Production of methanethiol from dimethylsulfoniopropionate in marine surface waters, Marine Chemistry, 54, 69–83, https://doi.org/10.1016/0304-4203(96)00006-0, 1996.

Kiene, R. P. and Linn, L. J.: The fate of dissolved dimethylsulfoniopropionate (DMSP) in seawater: tracer studies using 35S-DMSP, Geochimica et Cosmochimica Acta, 64, 2797–2810, https://doi.org/10.1016/S0016-7037(00)00399-9, 2000.

Kilgour, D. B., Novak, G. A., Sauer, J. S., Moore, A. N., Dinasquet, J., Amiri, S., Franklin, E. B., Mayer, K., Winter, M., Morris, C. K., Price, T., Malfatti, F., Crocker, D. R., Lee, C., Cappa, C. D., Goldstein, A. H., Prather, K. A., and Bertram, T. H.: Marine gas-phase sulfur emissions during an induced phytoplankton bloom, Atmos. Chem. Phys., 22, 1601–1613, https://doi.org/10.5194/acp-22-1601-2022, 2022.

Kilgour, D. B., Novak, G. A., Claflin, M. S., Lerner, B. M., and Bertram, T. H.: Production of oxygenated volatile organic compounds from the ozonolysis of coastal seawater, Atmos. Chem. Phys., 24, 3729–3742, https://doi.org/10.5194/acp-24-3729-2024, 2024.

Latorre, M. P., Iachetti, C. M., Schloss, I. R., Antoni, J., Malits, A., De La Rosa, F., De Troch, M., Garcia, M. D., Flores-Melo, X., Romero, S. I., Gil, M. N., and Hernando, M.: Summer heatwaves affect coastal Antarctic plankton metabolism and community structure, Journal of Experimental Marine Biology and Ecology, 567, 151926, https://doi.org/10.1016/j.jembe.2023.151926, 2023.

Lawson, S. J., Law, C. S., Harvey, M. J., Bell, T. G., Walker, C. F., De Bruyn, W. J., and Saltzman, E. S.: Methanethiol, dimethyl sulfide and acetone over biologically productive waters in the southwest Pacific Ocean, Atmos. Chem. Phys., 20, 3061–3078, https://doi.org/10.5194/acp-20-3061-2020, 2020.

McParland, E. L. and Levine, N. M.: The role of differential DMSP production and community composition in predicting variability of global surface DMSP concentrations, Limnology & Oceanography, 64, 757–773, https://doi.org/10.1002/lno.11076, 2019.

Mynard, C., Franklin, E. B., Alroe, J., Somerville, N., Patti, A., Siems, S. T., Williams, A., Mallet, M. D., Humphries, R., and Dunne, E.: Constraining Atmospheric Methanethiol Estimates Over the Southern Ocean, Geophysical Research Letters, 52, e2025GL116470, https://doi.org/10.1029/2025GL116470, 2025.

Novak, G. A., Kilgour, D. B., Jernigan, C. M., Vermeuel, M. P., and Bertram, T. H.: Oceanic emissions of dimethyl sulfide and methanethiol and their contribution to sulfur dioxide production in the marine atmosphere, Atmos. Chem. Phys., 22, 6309–6325, https://doi.org/10.5194/acp-22-6309-2022, 2022.

Rocco, M., Dunne, E., Peltola, M., Barr, N., Williams, J., Colomb, A., Safi, K., Saint-Macary, A., Marriner, A., Deppeler, S., Harnwell, J., Law, C., and Sellegri, K.: Oceanic phytoplankton are a potentially important source of benzenoids to the remote marine atmosphere, Commun Earth Environ, 2, 175, https://doi.org/10.1038/s43247-021-00253-0, 2021.

Rocco, M., Dunne, E., Peltola, M., Barthelmeß, T., Salignat, R., Chamba, G., Saint-Macary, A., Barr, N., Safi, K., Marriner, A., Deppeler, S., Harnwell, J., Engel, A., Colomb, A., Saiz-Lopez, A., Law, C. S., and Sellegri, K.: Fluxes of Biogenic and Oxygenated VOCs From In Situ Mesocosm Studies of Seawaters From the South-West Pacific Ocean, JGR Atmospheres, 130, e2024JD043056, https://doi.org/10.1029/2024JD043056, 2025a.

https://doi.org/10.5194/egusphere-2026-1720
Preprint. Discussion started: 8 April 2026

Rocco, M., Dunne, E., Salignat, R., Saint-Macary, A., Peltola, M., Barthelmeß, T., Chamba, G., Barr, N., Safi, K., Marriner, A., Deppeler, S., Rose, C., Uitz, J., Harnwell, J., Engel, A., Colomb, A., Saiz-Lopez, A., Harvey, M. J., Law, C. S., and Sellegri, K.: Relating Dimethyl Sulphide and Methanethiol Fluxes to Surface Biota in the South-West Pacific Using Shipboard Air-Sea Interface Tanks, JGR Atmospheres, 130, e2024JD041072, https://doi.org/10.1029/2024JD041072, 2025b.

Salignat, R., Rose, C., Banson, S., Berthet, S., Lupascu, A., Uitz, J., Mallet, M., Seferian, R., Rocco, M., Colomb, A., Dunne, E., Saint-Macary, A., Marriner, A., Law, C. S., and Sellegri, K.: Sensitivity Study of Atmospheric DMS Simulated in WRF-Chem to Various Oceanic DMS Fields Over the South West Pacific, JGR Atmospheres, 130, e2024JD042271, https://doi.org/10.1029/2024JD042271, 2025.

Sallée, J.-B., Pellichero, V., Akhoudas, C., Pauthenet, E., Vignes, L., Schmidtko, S., Garabato, A. N., Sutherland, P., and Kuusela, M.: Summertime increases in upper-ocean stratification and mixed-layer depth, Nature, 591, 592–598, https://doi.org/10.1038/s41586-021-03303-x, 2021.

Sander, R.: Compilation of Henry's law constants (version 5.0.0) for water as solvent, Atmos. Chem. Phys., 23, 10901–12440, https://doi.org/10.5194/acp-23-10901-2023, 2023.

Sellegri, K., Harvey, M., Peltola, M., Saint-Macary, A., Barthelmeß, T., Rocco, M., Moore, K. A., Cristi, A., Peyrin, F., Barr, N., Labonnote, L., Marriner, A., McGregor, J., Safi, K., Deppeler, S., Archer, S., Dunne, E., Harnwell, J., Delanoe, J., Freney, E., Rose, C., Bazantay, C., Planche, C., Saiz-Lopez, A., Quintanilla-López, J. E., Lebrón-Aguilar, R., Rinaldi, M., Banson, S., Joseph, R., Lupascu, A., Jourdan, O., Mioche, G., Colomb, A., Olivares, G., Querel, R., McDonald, A., Plank, G., Bukosa, B., Dillon, W., Pelon, J., Baray, J.-L., Tridon, F., Donnadieu, F., Szczap, F., Engel, A., DeMott, P. J., and Law, C. S.: Sea2Cloud: From Biogenic Emission Fluxes to Cloud Properties in the Southwest Pacific, Bulletin of the American Meteorological Society, 104, E1017–E1043, https://doi.org/10.1175/BAMS-D-21-0063.1, 2023.

Shaw, D. K., Sekar, J., and Ramalingam, P. V.: Recent insights into oceanic dimethylsulfoniopropionate biosynthesis and catabolism, Environmental Microbiology, 24, 2669–2700, https://doi.org/10.1111/1462-2920.16045, 2022.

Sieracki, M. E., Johnson, P. W., and Sieburth, J. M.: Detection, enumeration, and sizing of planktonic bacteria by image-analyzed epifluorescence microscopy, Appl Environ Microbiol, 49, 799–810, https://doi.org/10.1128/aem.49.4.799-810.1985, 1985.

Simó, R.: Production of atmospheric sulfur by oceanic plankton: biogeochemical, ecological and evolutionary links, Trends in Ecology & Evolution, 16, 287–294, https://doi.org/10.1016/S0169-5347(01)02152-8, 2001.
Stefels, J., Steinke, M., Turner, S., Malin, G., and Belviso, S.: Environmental constraints on the production and removal of the climatically active gas dimethylsulphide (DMS) and implications for ecosystem modelling, Biogeochemistry, 83, 245–275, https://doi.org/10.1007/s10533-007-9091-5, 2007.

Sun, J., Todd, J. D., Thrash, J. C., Qian, Y., Qian, M. C., Temperton, B., Guo, J., Fowler, E. K., Aldrich, J. T., Nicora, C. D., Lipton, M. S., Smith, R. D., De Leenheer, P., Payne, S. H., Johnston, A. W. B., Davie-Martin, C. L., Halsey, K. H., and Giovannoni, S. J.: The abundant marine bacterium Pelagibacter simultaneously catabolizes dimethylsulfoniopropionate to the gases dimethyl sulfide and methanethiol, Nat Microbiol, 1, 16065, https://doi.org/10.1038/nmicrobiol.2016.65, 2016.

Vaqué, D., Berdalet, E., Sotomayor-Garcia, A., Estrada, M., Cabrera-Brufau, M., Masdeu-Navarro, M., Rocchi, A., López-Alforja, X., Vila, M., Marrasé, C., Simó, R., Dall'osto, M., and Sala, M. M.: Assessing the relationship between viruses and protists and their role in dimethylsulphoniopropionate release in Antarctic surface microlayers, Antarctic Science, 37, 265–277, https://doi.org/10.1017/S0954102025100205, 2025.

https://doi.org/10.5194/egusphere-2026-1720
Preprint. Discussion started: 8 April 2026

Vaulot, D., Courties, C., and Partensky, F.: A simple method to preserve oceanic phytoplankton for flow cytometric analyses, Cytometry, 10, 629–635, https://doi.org/10.1002/cyto.990100519, 1989.

Willeke, K. and Baron, P. A.: Aerosol measurement: principles, techniques, and applications, Van Nostrand Reinhold, New York, 1993.

Wohl, C., Villamayor, J., Galí, M., Mahajan, A. S., Fernández, R. P., Cuevas, C. A., Bossolasco, A., Li, Q., Kettle, A. J., Williams, T., Sarda-Esteve, R., Gros, V., Simó, R., and Saiz-Lopez, A.: Marine emissions of methanethiol increase aerosol cooling in the Southern Ocean, Sci. Adv., 10, eadq2465, https://doi.org/10.1126/sciadv.adq2465, 2024.

Wohl, C., Williams, L. R., Deschaseaux, E., Quéléver, L. L. J., Beddows, D. C. S., Stark, H., Pospisilova, V., Lopez-Hilfiker, F., Chamba, G., Sellegri, K., Sà, E. L., Güell-Bujons, Q., Vila, M., Castillo, Y. M., Rocchi, A., Sotomayor, A., Vaqué, D., Dall'Osto, M., Berdalet, E., and Simó, R.: Methanethiol and dimethyl sulfide measurements in seawater and the atmosphere around the Antarctic Peninsula and in the Weddell Sea, https://doi.org/10.5194/egusphere-2026-1472, 20 March 2026.

Yentsch, C. S. and Menzel, D. W.: A method for the determination of phytoplankton chlorophyll and phaeophytin by fluorescence, Deep Sea Research and Oceanographic Abstracts, 10, 221–231, https://doi.org/10.1016/0011-7471(63)90358-9, 1963.